
MIRUS
Marvelous. In Every Way.

Institute for Aeronautics and Astronautics
Department of Aircraft Design and Aerostructures
Prof. Dr.-Ing. A. Bardenhagen

Joint NASA / DLR Aeronautics Design Challenge 2019

MIRUS

Team

Beck, Ramón
Cabac, Yannic
Dehmel, Jiri
Fritzsche, Felix
Kracke, Lennart
Lehnhardt, Kevin
Miertsch, Kristof
Roscher, Stephanie
Uzun, Roman
Vo, Ai Quynh

Academic Support and Advisors

M.Sc. A. Gobbin
Prof. Dr.-Ing. A. Bardenhagen

Submitted on July 1st, 2019

"[...] beyond the horizon of urban clutter there is a Great Land beneath our flag that can provide a new tomorrow for this century's 'huddled masses yearning to be free'".

Richard Peter (about Alaska's state motto "North to the Future")

Table of Contents

List of Figures . . . . . **VIII**

List of Tables . . . . . **IX**

Nomenclature . . . . . **X**

Meet the Team behind MIRUS . . . . . **XV**

1 Think beyond Technology **1**

2 Requirements **3**
2.1 Aiming for the Goals 3
2.2 Peerless Operational Versatility 3

3 A Sophisticated Design **5**
3.1 Three Surface Configuration 5
3.2 High-Lift Devices 5
3.3 Powerplant 6
3.4 Engine Placement 6
3.5 In Sync with Market Requirements 7

4 Autonomy **10**
4.1 Gradual Phasing-In 10
4.2 Pre-Programmed Sequences 11
4.3 Autonomous Environmental Perception and Recognition System 11
4.4 Resilience Planning 12
4.5 Assimilation to Existing System 12

5 Aircraft Characteristics **13**
5.1 Design Algorithm 13
5.2 Performance 13
5.3 Propulsion System 17
5.4 Configurational Sizing 18
5.5 Powerplant Sizing 20
5.6 Lighter by Design 21

6 Optimization to the Core **22**
6.1 Noise 22
6.2 DOC 22
6.3 Degree of Compliance 24

7 Conclusion **25**

Appendix . . . . . **XVI**

References . . . . . **XXIV**

List of Figures

2.1 Alaska route map . . . 3
2.2 Altitude analysis for ICA . . . 3
2.3 Time case study . . . 4
2.4 Mission plan . . . 4
3.5 Cross section view CCW . . . 6
3.6 MIRUS' serial hybrid scheme . . . 6
3.7 Fuselage group . . . 7
3.8 Economy, business and cargo cabin layout . . . 8
3.9 TAT procedures for PAX and cargo mission . . . 9
4.10 Road network to autonomy . . . 10
4.11 Communications network . . . 12
5.12 MIRUS' design algorithm . . . 13
5.13 Mission profile . . . 14
5.14 Thrust matching for Mission (B) at ISA MSL . . . 14
5.15 ROC for Mission (A) . . . 15
5.16 ROD for Mission (A) . . . 16
5.17 Effect chain of the propulsion system . . . 17
5.18 Propeller diameter sizing . . . 17
5.19 Wing planform and lift coefficient distribution . . . 18
5.20 Stability and control diagram . . . 20
5.21 Energy and fuel mass breakdown for Mission (A)/(B) . . . 20
5.22 Mass breakdown for Mission (A)/(B) . . . 21
6.23 Peak noise contours during take-off . . . 22
6.24 Unit cost of MIRUS . . . 23
6.25 Break-even analysis . . . 23
6.26 Direct operating costs per seat mile . . . 24
6.27 Compliance check . . . 24
C.1 Cabin cross-section . . . XIX
D.1 Cascaded sequence run . . . XX
E.1 Energy consumption (above) and SOC (below) for Mission (A) . . . XXI
E.2 Energy consumption (above) and SOC (below) for Mission (B) . . . XXI

List of Tables

5.1 Take-off performance data for Mission (B) . . . 14
5.2 Climb performance data for Mission (A) . . . 15
5.3 Cruise performance data . . . 16
5.4 Descent performance data for Mission (A) . . . 16
5.5 Landing performance data for Mission (B) . . . 16
5.6 Electric engine parameters . . . 17
5.7 Wing parameters . . . 18
5.8 CCW parameters . . . 19
5.9 Empennage data . . . 20
5.10 Powerplant data for Mission (B) . . . 20
5.11 Basic mass breakdown for PAX version . . . 21
6.12 Simulated A/C noise (MP) . . . 22
6.13 Comparison of block-hour costs . . . 24
A.1 List of key technologies . . . XVII
C.1 Cabin parameters . . . XIX
F.1 Detailed mass breakdown . . . XXII
G.1 Technical data sheet . . . XXIII

Nomenclature

Latin Symbols

Symbol	Unit / Definition	Designation
C	$1/h$, -	Charging rate, coefficient
D	N, m	Drag, diameter
E	Wh	Energy
E/m	$\mathrm{Wh/kg}$	Specific energy (energy density)
M	-	Mach number
P	W	Power
P/m	$\mathrm{W/kg}$	Specific power (power density)
S	m^2	Area
T	N	Thrust
T/W	-	Specific thrust (thrust to weight ratio)
W	N	Weight
W/S	$\mathrm{N/m^2}$	Wing loading
V	$\mathrm{km/h}$	Velocity
b	m	Span
c	m	Chord
c_p	$\mathrm{J/kgK}$	Specific heat capacity
e	-	Oswald efficency number
g	9.80665 $\mathrm{m/s^2}$	Gravity
m	kg	Mass
$\dot{m}$	$\mathrm{kg/s}$	Massflow
q	$\rho/2$ V^2	Dynamic pressure
r_H	m	Distance neutral point wing to neutral point VT
w	$\mathrm{m/s}$	Rate of climb / descent
x_{NFR}	m	Distance CG to wing neutral point

Greek Symbols

Symbol	Unit	Designation
α	$^\circ$	Angle Of attack
ρ	$\mathrm{kg/m^3}$	Density
η	-	Efficiency
ϵ	$^\circ$	Installation angle
γ	$^\circ$, -	Flight path angle, dimensionless circulation
ϕ	$^\circ$	Sweep angle
Λ	-	Aspect ratio
λ	-	Taper ratio
Π	-	Compressor pressure ratio

Indizes

Symbol	Designation
app	Approach
CAR	Cargo
CCW	Circulation Control Wing
CL	Climb
CR	Cruise
CMP	Compressor
D	Drag
DS	Descent
el	Electric
F	Fuel
g	Gravity Force
GEN	Generator
GND	Ground
ICA	Initial Cruise Altitude
ICL	Initial Climb
L	Lift
LDG	Landing
max	Maximum
mec	Mechanical
MTOM	Maximum Take-Off Mass
P	Power
Prop	Propeller
R	Range
ref	Reference
TO	Take-Off
tot	Total
W	Wing
∞	Inflow
μ	Momentum
0	Zero lift

Abbreviations

Abbreviation	Designation
A/C	Aircraft
AESA	Active Electronically Scanned Array
AEPRS	Autonomous Environmental Perception and Recognition System
ALT	Alternate
ANOPP	Aircraft Noise Prediction Program
AOA	Angle of Attack
AOCO	Airline Operational Center Operator
APP	Approach
ASAP	As Soon As Possible
ATC	Air Traffic Control
ATCO	Air Traffic Control Operator
AVBL	Available
BAT	Battery
BHC	Block-Hour Costs
CAP	Supercapacitor
CCW	Circulation Control Wing
CESTOL	Cruise Efficient Short Take-Off and Landing
CFR	Code of Federal Regulations
CG	Center of Gravity
CLNC	Clearance
CW	Canard Wing
DEW	Delivery Empty Weight
DOC	Direct Operating Costs
EVS	Enhanced Vision System
FAA	Federal Aviation Administration
FCA	Final Cruise Altitude
FL	Flight Level
FPD	Flights Per Day
FT	Flight Time
GEN	Generator
GO	Ground Operator
GPS	Global Positioning System
GSAAS	Ground Supervised Autonomous Aircraft System
GSE	Ground Support Equipment
HLD	High-Lift Devices
HT	Horizontal Tail
ISA	International Standard Atmosphere
ICA	Initial Cruise Altitude

KIAS	Knots Indicated Airspeed
LFL	Landing Field Length
LGF	Lift-Gain-Factor
MBS	Mean Block Speed
MCL	Mount McKinley Airport
MIRUS	Multifaceted Intelligent Rural to Urban Shuttle
MP	Measurement Point
MSL	Mean Sea Level
MSN	Mission
MTOM	Maximum Take-Off Mass
NACA	National Advisory Committee for Aeronautics
NASA	National Aeronautics and Space Administration
OANS	On-Board Airport Navigation System
OEM	Operation Empty Mass
OLED	Organic Light Emitting Diode
PAX	Passengers
REG	Regular
REQS	Requirements
ROC	Rate Of Climb
ROD	Rate of Descent
RPAS	Remotely Piloted Aircraft System
RPM	Revolutions Per Minute
RQD	Required
SET	Specific Excess Thrust
SFC	Specific Fuel Consumption
SMC	Seat Mile Cost
SOC	State Of Charge
SOP	Standard Operating Procedures
SPL	Sound Pressure Level
SPO	Single-Pilot Operations
STOL	Short Take-Off and Landing
TAT	Turn-Around Time
TCAS	Traffic Alert and Collision Avoidance System
TLAR	Top Level Aircraft Requirement
TOFL	Take-Off Field Length
TRL	Technological Readiness Level
TSA	Three Surface Aircraft
VT	Vertical Tail
VTOL	Vertical Take-Off and Landing
ZFM	Zero Fuel Mass

Meet the Team behind MIRUS

Ramón Beck

Yannic Cabac

Jiri Dehmel

Felix Fritzsche

Lennart Kracke

Responsible For Making The Magic Happen

Kevin Lehnhardt

Kristof Miertsch

Stephanie Roscher

Roman Uzun

Ai Quynh Vo

1 Think beyond Technology

mirus (latin) ['miːrʊs] (*verb*) | Marvelous, amazing, surprising.

Nowadays 55 percent of the world's population live in urban areas. With an 80 percent urban population, the United States of America ranks among the most urban countries in the world. According to the US Census Bureau, urban areas are defined as territories with a population density of at least 500 persons per square mile and more than 2,500 inhabitants [1]. Conversely, this means that about 20 percent of the US population live in rural areas, which are classified as "any population, housing, or territory not in an urban area" [2]. These approximately 60 million people are scattered across 97 percent of the country [3]. At county level, rural areas are subdivided into Metropolitan Statistical Areas (metro areas) and nonmetro areas. Whereas metro areas (inhabited by 54.4 percent of rural people) offer a high degree of economic and social integration with adjacent urban areas, the approximately 30 million inhabitants of nonmetro areas are severely cut off from civilization [4]. The consequences of such isolation are numerous and range from insufficient medical care to a lack of academic and economic opportunities [5]. Alaska, as the largest state in the USA, is exposed to the consequences of deficient medical care. One third of the people living in rural areas have no direct access to rural health clinics [6] [7]. Due to the fact that more than 80 percent of the communities are not connected to the road network, the connection to the few existing clinics is not ensured [8]. Thus, significant migration from rural areas to cities has been recorded in recent years [9].

By 2050, two thirds of the world's population will live in urban areas [10]. Worldwide urbanization is the main driver of economic growth and is therefore a characteristic of urban development, especially in the emerging markets [11]. These markets are characterized not only by a flourishing, vibrant economy but above all by large population growth. For example, India will become the world's largest population by 2050 with a current birth rate of 2.5 children per woman [12]. Consequently, the rapidly growing middle class is creating a strong need for mobility, which has a number of significant advantages, such as access to jobs and individual freedom [13] [14]. As a result, 200 million people will flock to work and live in urban centers over the next 15 years [15].

Although urbanization increases productivity and improves the gross domestic product per capita in the long term, it also causes considerable pressure in those urban centers. For example, the existing urban infrastructure cannot support such an increase in the number of vehicles on the road, resulting in almost half of all city drivers spending more than 12 hrs a week in the car. Strong immigration will further increase the proportion of the urban population living in slums to 24 percent [16].

A lack of or inadequate infrastructure is therefore not only a problem for established markets (such as the USA), but will also challenge emerging markets in the future. The inherent dynamics of urban development tend to make cities the main drivers for achieving the Sustainable Development Goals. These thematically diversified targets consider social as well as economic and especially ecological aspects. They are intended as a call for action to all United Nation member states and aim at promoting prosperity and protecting the planet at the same time. Establishing high-quality, reliable and resilient infrastructure, both regional and cross-border, is one of the major elements in achieving these objectives by 2030 [16].

Particularly on shorter distances, this infrastructural connection usually involves ground-based transport by bus, car, truck or train. Aside from economic advantages, ground transport has various inherent disadvantages. The ground-based access to new areas is highly dependent on topographical conditions. Mountains and waters require the construction of tunnels and bridges, which is not only time-consuming but also cost-intensive. It should be noted that there are areas which cannot be made accessible by ground-based routes. In order to create a reliable infrastructure, a dense road network is required, which can cause a variety of environmental problems. These range from soil sealing to the progressive deforestation of adjacent forests [17].

Therefore, the ultimate solution is an aircraft operating independently of the topographical conditions and landing at precisely defined locations in order to keep the ecological footprint as low as possible. Admittedly, flight operations are not entirely independent of the corresponding infrastructure, but relatively short runways that are not necessarily paved are sufficient for commuter

aircraft. This infrastructure already exists in many areas. In order to enable efficient, economical flight operations even on short routes, a tremendous degree of flexibility and high utilization must be guaranteed. As this is not achieved in an economic way with current aircraft and operating concepts, the Essential Air Service Program was established to make these routes to rural airports more attractive. With its 520 airports, Alaska already provides a dense network of subsidized infrastructure. In order to place a successful and competitive design, it is mandatory to consider the entire traffic concept and analyze its future evolution. Nowadays, traffic in many cities (and nearly all outskirts and rural areas) necessitates individual vehicle ownership - alternative options are either deficient or simply not existent - causing pollution and traffic congestion. To overcome this massive inefficiency, entirely new means of transport must be introduced today to transform public and private transport in cities [18]. Hence, reliable implementation of multi- and intermodal transport systems is the key to fully exploit the benefits of mobility transformation. In the upcoming years, the trend towards urban mobility will be fueled primarily by three main drivers: increasing electrification, autonomy and displacement into the air [19]. Automated flight control and navigation systems have been standard in aviation since the 1970s. Air transport is therefore far better suited to autonomy in comparison to the automotive industry, which is still in its infancy [20].
Over the long term, the implementation of new inner-city airports to connect urban traffic to conventional airports is imperative. These so-called "CentAirStations" enable the handling and distribution of passengers and cargo between different modes of transport, e.g. train and plane, in a multi-level building, allowing very short processing times [21]. In order to empower those urban multimodal solutions, a holistic approach includes the use of commuter aircraft, currently ensuring the connection of remote areas to the urban infrastructure and, in the long term, enabling the connection to the transit points described above.

The purpose of this design study is to present a valid preliminary versatile aircraft concept with entry into service in 2025, using a wide range of promising technologies and leading in a new commuter era. Alternative powerplant concepts, a highly flexible mission management and optimized, autonomous aircraft operations shall be taken into consideration.
It is mandatory to determine the needs of future markets in order to develop a sustainable and successful concept. Therefore, the elaborated unique, flexible design is based on both a market analysis and a technology outlook. To validate a sustainable integration into the overall air traffic system, the operational concept is subjected to a feasibility study, which shall help identifying solution approaches to possible challenges. Due to this analysis, the top level aircraft requirements of the present design are defined aiming further detailing in the progressive development process. With the help of relevant literature and established calculation methods, several configurations have been elaborated. However, only the final results refined in several iterations are presented. Assessing the competitiveness of the design and the degree of compliance, the sustainability of the concept is finally evaluated from different perspectives.

Focused on the optimal use of synergy effects to fully unlock the potential of future commuter markets, the following sections present the concept of MIRUS.

Multifaceted **I**ntelligent **R**ural to **U**rban **S**huttle.

2 Requirements

The design space is limited on the one hand by legal regulations and on the other by economic factors. In order to optimize the design with regard to all aspects, initial requirements, including general and Top Level Aircraft Requirements (**TLAR**s), have to be prioritized and goals must be set, followed by the introduction of the sophisticated concept of operation.

2.1 Aiming for the Goals

MIRUS is able to transport **nine passengers** including their luggage or **2,000 lbs of cargo**, respectively. Hence, the certification as commuter class is in accordance with the guidelines. Beside the **operational range of 120 NM**, a **maximum range of 500 NM** is targeted. Alaska is a potential operation site which thus can be covered optimally by the selected maximum range (see Figure 2.1). All ranges need to be achieved within **less than 99 min** due to the exclusion of service facilities on board. The **speed** is derived from a time case study in the following Subsection.
With a **minimum Inital Cruise Altitude of 10,000 ft**, MIRUS is capable of passing most of the earth's obstacles while avoiding the speed limit of 250 KIAS. In addition, Northern Americas topologic chart (see Figure 2.2) points out that the core market can be served completely.

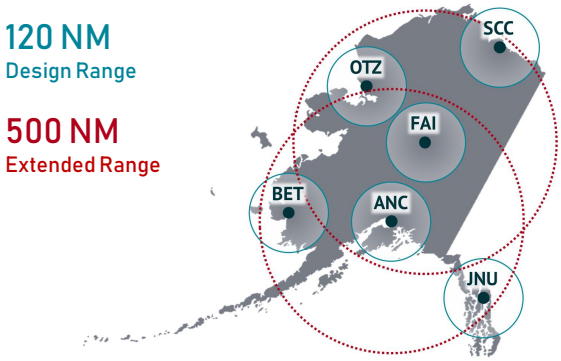

Figure 2.1: Alaska route map

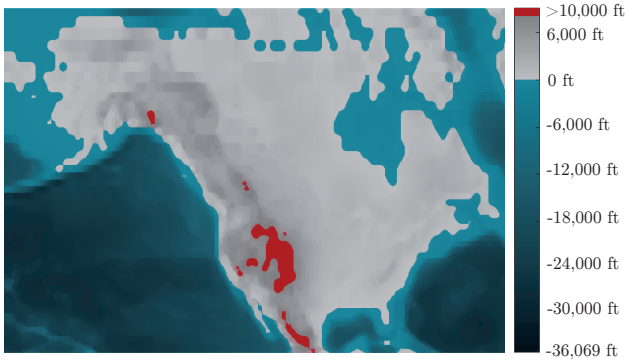

Figure 2.2: Altitude analysis for ICA

Furthermore, a diversion range of 100 NM is intended which corresponds to 20 percent of the maximum range. More flexibility regarding the choice of alternates is also given in sparsely populated areas. With a minimum required take-off and landing field length of 1,000 ft, MIRUS can operate at the majority of airports in the world, as 98 percent have longer runways [22]. To ensure lead-free missions, aviation kerosene type JET-A1 is chosen [23]. In addition, JET-A1 has a very high availability at airports in the world, which guarantees a flexible operation of MIRUS [24]. As shown in the mission plan (see Figure 2.4), the aircraft is also operating at critical times concerning noise emissions. Therefore, a noise level as low as possible is aimed. The overall goal is to achieve minimum operating costs. The degree of compliance is summarized in Subsection 6.3.

2.2 Peerless Operational Versatility

A highly performant system, such as MIRUS, requires a sophisticated mission plan and operational concept to deliver the economical benefits it is capable of. However, certification regulations (14 CFR §23, §135) and design requirements also need to be considered in order to achieve a feasible design.

2.2.1 Mission Plan

The mission plan consists of a sequence of Passenger (PAX) and cargo missions over one operation day. Initially, the attended Flight Time (FT) and thus the Mean Block Speed (MBS) are determined. Both parameters derive from the PAX mission as it is limited in the maximum flight time. The comparison of different flight times results in three potential mission scenarios with an even number of Flights Per Day (FPD) (see Figure 2.3).

Case C is selected due to the following reasons:

- The short FT of 27 min leads to a higher economical attractiveness for passengers and thus to a higher capacity utilization (see Section 1).
- The high number of ten FPD decreases the seat mile costs significantly (see Section 6) in order to achieve the main goal of being exceptionally economical.
- The high MBS enables to reach the targeted maximum range of 500 NM (see Subsection 5.2).

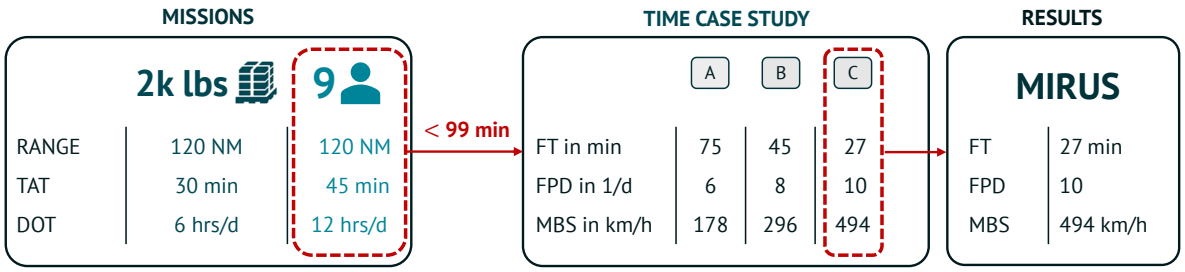

Figure 2.3: Time case study

Apart from the flight time, the ground time must also be taken into consideration. Therefore, a detailed schedule over the day is created (see Figure 2.4). As commuter air service is part of the customers' transport chain, the mission plan is synchronized with their daily commuter behavior. More than 80 percent of the target group depart before 0859 L travelling a mean distance of 166.4 miles in an average time of 119 min [25]. However, the sophisticated schedule of MIRUS is designed to suite the passengers demands with a reduced trip time of 27 min. Additionally, cargo missions are proceeded around midday due to low passenger demand. Consequently, less cargo flights are carried out during night time resulting in less night surcharges. Subsequently, the commuter service is resumed before the remaining freight missions are carried out. A two hour break is scheduled at the end of each operating day to conduct light maintenance or servicing.

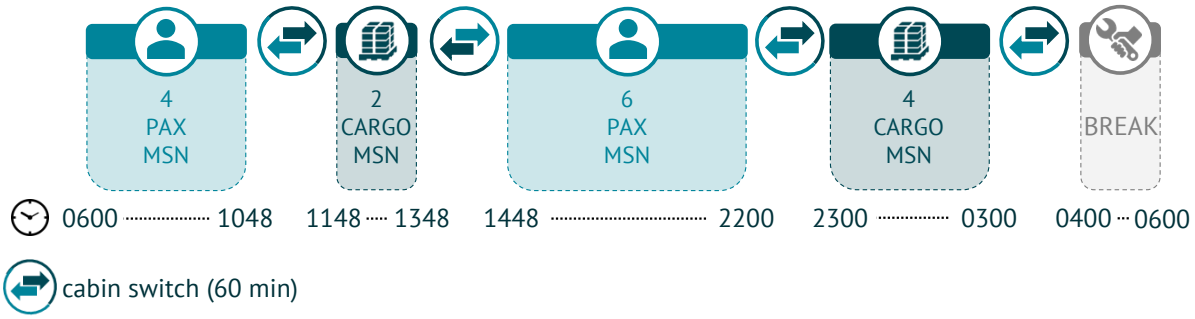

Figure 2.4: Mission plan

2.2.2 Operational Concept

On the design mission, MIRUS is operating at a capacity of 300 full revenue days per year. Based on the mission plan, this results in seven and a half flight hours per day. Besides an annual inspection, 14 CFR §91.409 requires an inspection every 100 flight hrs. Hence, this check is carried out every 13 days. This accumulates a total amount of 24 maintenance days per year, assuming both the 100 hour check and annual inspection taking a day of maintenance [26]. During the remaining 41 days MIRUS can be used for training purposes, charter flights or other tasks.

3 A Sophisticated Design

MIRUS is a pressurized, multi-engine, three lifting surfaces aircraft powered by a serial plug-in hybrid-electric propulsion system and fully compliant to 14 CFR §23, § 135. The multimodular cabin provides space for either nine passengers in standard cabin layout or 2,000 lbs of cargo. A market analysis reveals particularly short runways as well as exceptional efficiency and transport performance to be crucial benchmarks. Therefore, this concept is driven by a powerful propulsion system and an innovative high-lift configuration. The following section offers an overview of used technologies and their implementation into the concept design. To ensure feasibility a Technological Readiness Level (TRL) of at least 7 is assumed. For each technology, the respective TRL is indicated. In addition, a detailed overview of all key technologies is provided in Appendix A. It should be noted that this is a preliminary draft to point out future solutions and thus forms the basis for more detailed concept studies.

3.1 Three Surface Configuration

The challenging TLARs regarding take-off and landing distance can only be met by a Short Take-Off and Landing (STOL) or Vertical Take-Off and Landing (VTOL) design. By using distributed electric propulsion, a number of previous challenges for VTOL designs like the power to weight ratio and the controllability can be solved. However, when scaled up, increasing battery weight due to rising energy and power demand for hovering will get more difficult to compensate [27]. Using STOL instead of VTOL allows a significant reduction in mass, which is highly desirable regarding fuel and cost efficiency. As indicated by the market analysis, potential approach destinations are indeed characterized by a reduced runway length, which is nevertheless perfectly sufficient for STOL, thus making the use of VTOL technology completely inefficient.

In order to achieve Cruise-Efficient, Short Take-Off and Landing (CESTOL) characteristics, the right choice of configuration is the key. A conventional design is a proven concept, however, the horizontal tail needs to generate a downforce. This leads to additional lift at the main wing and thus increased induced drag from the main wing and the horizontal stabilizer itself, which is known as trim drag [28]. A canard configuration is a potential solution to this problem, since the canard generates lift to keep the aircraft in equilibrium, reducing also main wing lift and induced drag [29]. For stability reasons, the canard needs to stall before the wing, resulting in a higher stall speed compared to wing only stall speed and thus prolonged take off and landing distances [29].

A Three Surface Aircraft (TSA - TRL 9) has the potential to incorporate the benefits of canard and conventional configurations regarding cruise efficiency and STOL performance at the cost of increased complexity [28]. Moreover, unlike a two lifting surface configuration, a TSA can reduce induced lift at any Center of Gravity (CG) position, offering more flexibility in cargo and passenger placement [30]. Due to these advantages, such a TSA configuration is used for MIRUS. To prevent damages during ground operations, the canard is designed to be foldable (TRL 8). The main wing is build as a shoulder wing in order to provide sufficient ground clearance for the wingtip mounted propellers (see Subsection 3.4). For the vertical and horizontal stabilizers a T-tail assembly is chosen: The end plate effect allows a more effective and thus smaller vertical tail [28]. A detailed technical drawing is provided in Appendix B.

3.2 High-Lift Devices

In addition to this configuration, sophisticated high-lift devices are also needed to meet the challenging TLARs regarding take-off and landing distance. The high wing loading resulting from the fast cruising speed leads to a high stall speed that cannot be reduced to acceptable values using conventional high-lift devices.

Commercial STOL operation with field distances of 1,000 ft must use powered lift devices [31]. Thus, the MIRUS design incorporates a Circulation Control Wing (CCW - TRL 8), which allows main wing lift coefficients up to 7.6 for fully attached flow using the Coanda effect [32]. Due to economically reasons, a maximum lift coefficient of approximately 4 is aimed. The CCW system consists of four

main parts (see Figure 3.5): a suction slot, a jet injection (blowing) slot, followed by a 15 percent chord simple-hinged Coanda flap at the upper surface and a compact compressor.
By injecting high momentum jet flow tangential to the stream at the upper surface hinge point, separation is delayed to larger angles of attack enabling larger maximum lift coefficients. The required pressurized air is provided by several redundant compact single-staged axial compressors located in the wing root. Suction slots stabilize the boundary layer and supply ram air to the compressor inlets. Another advantage over conventional fowler-flaps and leading-edge devices is the absence of disturbing obstacles like slats, which forces the boundary layer transition in cruise flight and, therefore, diminishing cruise efficiency.
The canard wing is equipped with additional conventional high-lift devices in order to guarantee controllability at the most forward CG position and balance out the excessive zero lift moment coefficient.

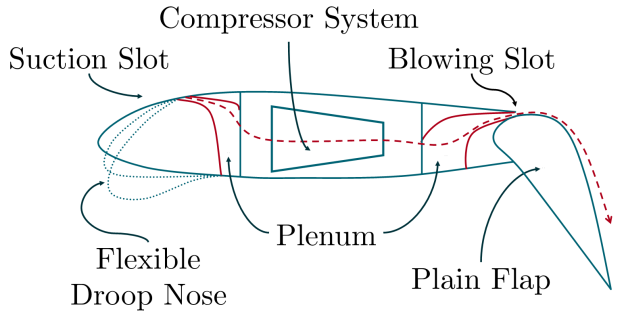

Figure 3.5: Cross section view CCW

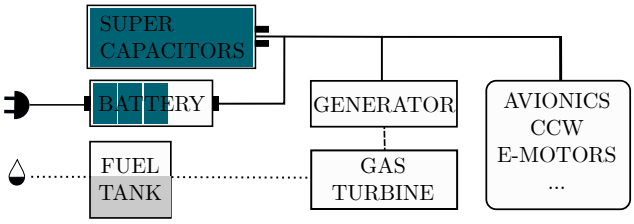

Figure 3.6: MIRUS' serial hybrid scheme

3.3 Powerplant

The use of electric propulsion systems (TRL 9) in aviation is still limited despite having numerous advantages over conventional systems. Electric motors have an excellent power to weight ratio and a small size [33]. Additionally, there is potential for noise emission and maintenance cost reduction [33]. Another benefit is the electric engine's astoundingly efficiency of 95 percent, giving an electric propulsion system roughly twice the energy efficency of conventional systems [34]. However, there is a serious drawback, namely the low gravimetric energy density of the energy storage systems. It is estimated that electric storage devices need an energy density of 500 $^{\mathrm{Wh}}/_{\mathrm{kg}}$ to fabricate commercially viable aviation products [35]. From the battery technologies available by 2025, advanced lithium-ion batteries (TRL 8) will deliver the highest energy density with 350 $^{\mathrm{Wh}}/_{\mathrm{kg}}$ at cell level, translating to around 235 $^{\mathrm{Wh}}/_{\mathrm{kg}}$ at pack level [36]. Another technology for storing electric energy are Lithium-Ion Capacitors (TRL 9). While lacking the energy density of batteries, they offer a better specific power density, making them suitable for covering peak power demands, e.g. on take-off or go-around [37]. Since MIRUS' battery is dimensioned by power demand, a reduction of mass is achieved using these Supercapcitors (CAP). Assuming that this technology is available, only a hybrid propulsion system would enable the use of electric motors at the cost of moderate increased weight and system complexity. For MIRUS, a serial hybrid system as depicted in Figure 3.6 is chosen, which offers fuel saving potential due to drag reduction from its configuration as explained in the following subsection [38]. Electric energy is stored in lithium-ion batteries and lithium-ion capacitors. A jet fuel driven gas turbine will be used in combination with an electric generator since it offers better power to weight ratio and reliability compared to an internal combustion engine [28]. Another alternative would be a hydrogen fuel cell, however, such a system currently lacks specific power and fuel availability.

3.4 Engine Placement

Due to the advantages explained in the previous chapter, electric motors can be positioned at locations that were unable to house conventional engines before. Placing the propulsion units at the wing tips (TRL 9) has multiple beneficial effects: Induced drag is reduced due to the wingtip

vortex and propeller wake interaction [39]. It is also possible to recover energy from the wingtip vortex, which leads to increased propeller efficiency and thus reduced engine power [39]. In case of asymmetric thrust in a single engine failure scenario, the excessive yaw moment must be compensated by an increased vertical tail area. Because of the tight TLARs regarding take-off distance, a third propulsion unit with a retractable propeller (TRL 7) is placed in the aft fuselage. This unit delivers additional thrust during take-off and climb and is stowed away in cruise to minimize drag. Moreover, it helps reducing the yaw moment in a single engine failure scenario and thus vertical tail size and drag.

3.5 In Sync with Market Requirements

Since the aircraft design process is an interaction of multiple aspects, a balance between passenger comfort, weight minimization and optimal utilization must be achieved for the interior design. Consequently, a flexible cabin arrangement is an integral component in order to transport the payload profitably.

3.5.1 Fuselage Group

In an effort of saving structure weight, and respecting the head strike radius of eight inch, the cabin is pressurized to maintain general breathing conditions at an altitude of 8,000 ft Mean Sea Level (MSL) and is thus designed in an elliptic shape. Cabin width extends to 54 inch while providing a cabin height of 6 inch (see Appendix C). The double-sided door is located on the fore left-hand side of the fuselage and is 55 inch high and 46 inch wide. It provides optimum access for passengers with a fuselage-integrated staircase, and opening both doors simplifies the transfer of cargo pallets. In order to ensure safe evacuations according to certification specifications, an emergency exit is located immediately opposite the main door on the right-hand side of the cabin. In the front section of the aircraft, components such as the radome, canard-wingbox, avionic compartment and cockpit are combined. To find a balance between utility, accessibility and centre of gravity in the positioning of the individual components, larger systems such as the landing gear well, the wingbox, the powerplant and the electric motor with propeller are positioned in the aft section (see Figure 3.7).

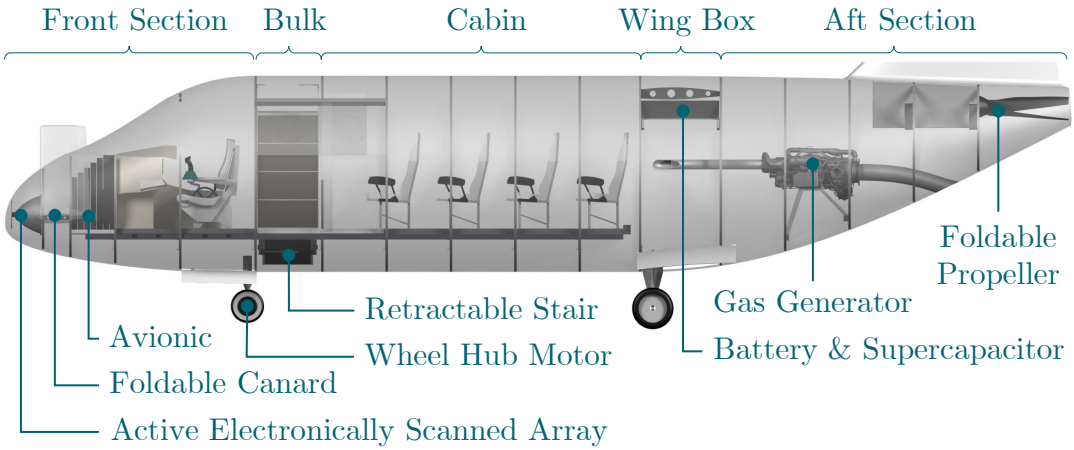

Figure 3.7: Fuselage group

3.5.2 Modular Cabin Design

In order to ensure a high utilization rate, the cabin layout is based on a modular pallet system (TRL 9) which makes it possible to realize an almost unlimited number of cabin configurations. Due to the configuration characteristics and because of weight-saving measures, a windowless design is implemented. With the purpose of avoiding any claustrophobic feeling or an uncomfortable condition on the part of the passenger, high fidelity OLED-displays (TRL 9) are embedded into the side wall showing images captured by a high-resolution outboard camera [40]. To protect the screens during cargo flights these are fitted with blinds.

Three elaborated cabin layouts are illustrated in Figure 3.8. MIRANDA, as the standard seating configuration, offers a capacity of nine seats with a width of 18 inch at 30 inch pitch, providing a certain standard of comfort even on short commuter flights. Designed for a luggage density of 175 $^{kg}/_{m^3}$ the bulk compartment is conveniently located after the entrance so that passengers can comfortably load their luggage before taking their seat. MIRUS offers not only the possibility to accommodate passengers, but also the opportunity of transporting 2,000 lbs of freight on specially designed pallets. For this purpose, each pallet made of an aluminum sandwich construction with an empty mass of 26.5 kg contributes (with a cargo density of 160 $^{kg}/_{m^3}$) a cargo volume of about 2.3 m^3 therefore 368 kg (including pallet mass). MIRUS' executive design MAYA also makes it an excellent alternative to a company-owned commuter aircraft with a comfortable four-seat configuration.

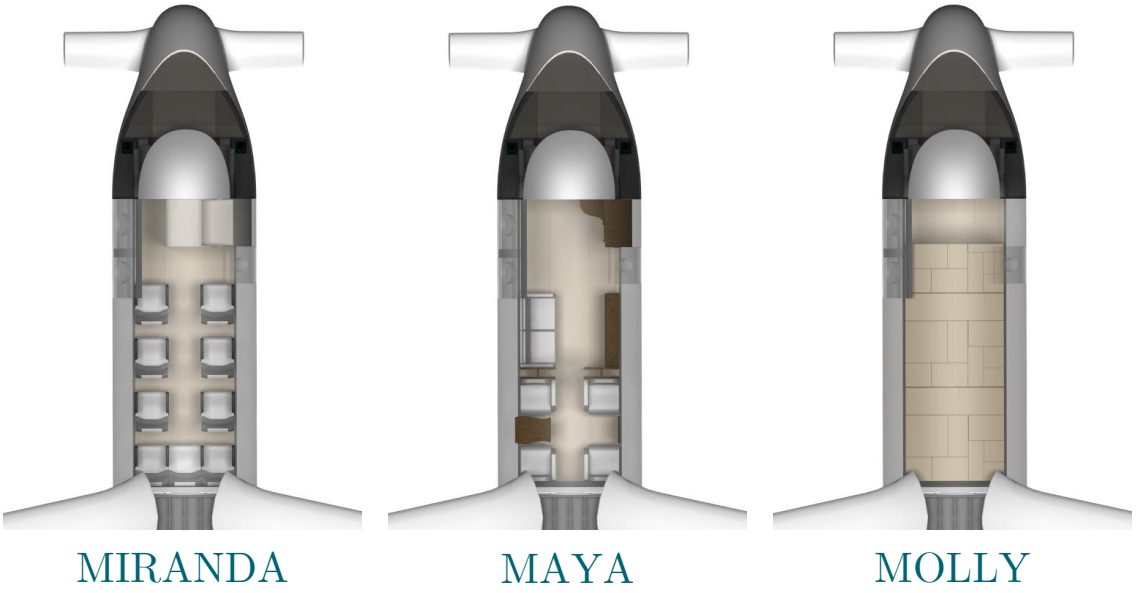

Figure 3.8: Economy, business and cargo cabin layout

3.5.3 Cabin Switch

The ban on night flights imposed on many airports applies to emission protection against night-time noise. However, there are exceptions for freight and postal flights.
In this case, it is possible to use MIRUS, non-usable for passenger flights during night time, for cargo transportation. This increases the effective flight time per day and thus results in higher yields to reduce costs (see Subsection 6.2). All individual components to be switched are stored on pallets to ensure a smooth daily changeover between passenger and freight flights [41]. Thanks to modular assembly, MIRUS is flexibly and innovatively prepared for any scenario. Especially in times of transition to autonomous flying the pilot arrangement will change in the following years of operation. For training purposes, a cockpit for two pilots will be required when the aircraft is fully loaded; in regular flight, one pilot will be operating in 2025, whereas the first remotely-piloted flights will be carried out with cargo (see Subsection 4). The desired pilot selection can be set up on a cockpit pallet and the three cabin pallets can be swapped from PAX to cargo configuration within 10 min, using a forklift truck. This allows the aircraft to comply with a cabin change within 60 min (see Section 2). Seat rails are integrated on each pallet, allowing variable configurations to be created. Via a vertical roller system at the wall and a horizontal one on the ground, the pallet can be rolled into the cabin centered and then be positioned and secured by bolts longitudinally to the flight direction. In summary, MIRUS offers the best conditions to follow the change of time with varying interior designs.

3.5.4 Ground Handling

Since the duration of ground handling processes largely depends on aircraft size, small commuter aircraft are usually characterized by short Turn-Around Times (TATs) with few standardized processes. Nevertheless, the 45 min specified in the present concept are absolutely reasonable, considering MIRUS' special design characteristic: the serial hybrid powerplant concept. The charging rate of a battery is directly related to its lifetime and thus a very long lifecycle is inevitably associated with a low charging speed (see Subsection 3.3). Due to this low charging speed, the reloading, assisted by the ground power unit, starts immediately after on-block prior to the passengers leaving the cabin. The already existing integrated power network at airports will be used with minor modifications to recharge the battery. A safety risk can be excluded as the aircraft is grounded [42]. As the remaining ground handling procedures do not differ significantly from the conventional ones, only brief attention will be paid in the following to the main features of the design. The greatest risk for an aircraft at airports is damage caused by mobile Ground Service Equipment (GSE) [43]. For this, the canard is folded up by 90 ° and the tail propeller is retracted during taxi-in. In order to reduce both noise and pollutant emissions, an electrically driven wheel hub motor (TRL 7) is used, which is integrated in the nose landing gear. This allows highly precise and smooth movement thanks to uninterrupted torque during the whole range of speed. This wheel hub motor and the integrated retractable lightweight staircase (TRL 9) enable MIRUS to be extremely flexible and independent from airport equipment and coordination. Besides avoiding delays (e.g. caused by waiting for the push-back), there is an immense financial saving potential, as there is no need to pay for passenger boarding bridges and mobile stair fees. In order to ensure seamless operation and prevent delays, an indispensable optimization of the turn-around process is achieved. Figure 3.9 shows all steps of the TAT which has been optimized to comply with the specified 45 min for passenger missions during daytime and 30 min for cargo missions. With its innovative modifications, MIRUS offers the best prerequisites to increase profitability and outperform competitors.

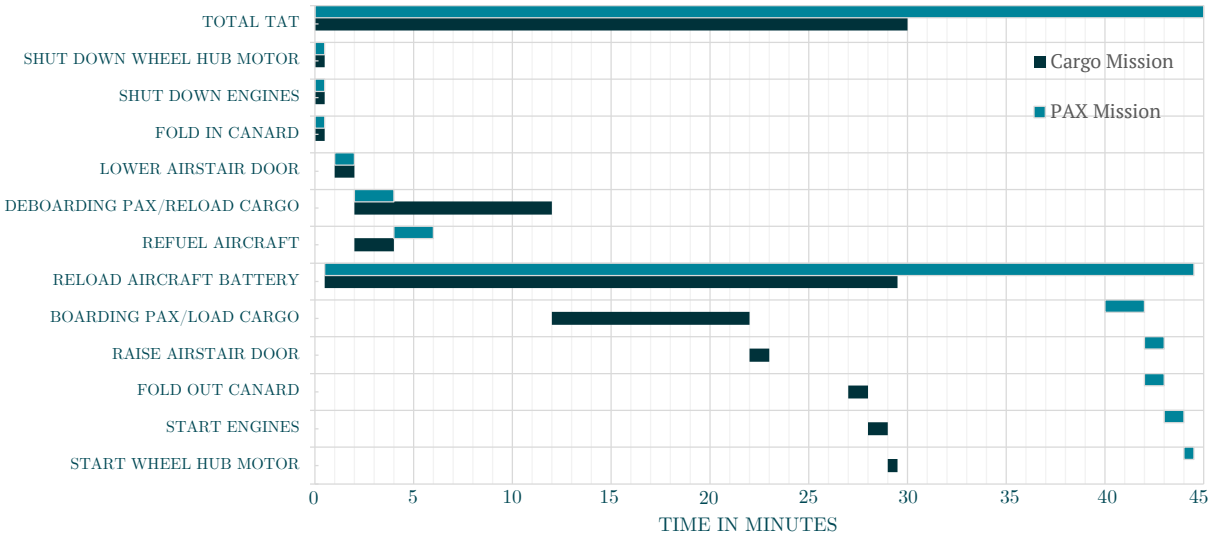

Figure 3.9: TAT procedures for PAX and cargo mission

4 Autonomy

With an average annual growth rate of 5 percent and a doubling of air traffic every 15 years, aviation faces an unmet annual demand of 17,000 pilots [44]. Considering up to 30 percent of an airline's total costs can be traced back to the crew, an enormous saving potential arises by reducing the number of pilots [45]. Furthermore, about 90 percent of aviation incidents and accidents can be attributed to human error [46]. Thus, the autonomous operation of commercial aircraft combines the priority safety of passengers and crews with the potential to reduce costs, increase efficiency and open up new missions [47]. Key challenges in the operation of autonomous aircraft comprise, among others, increased emphasis on security controls and efficient integration into the existing and future air traffic system. Coordinative bottlenecks can occur especially at highly frequented airports due to the enormous number of aircraft movements. However, this is of minor importance and will not be discussed in more detail as MIRUS is designed to connect remote areas and operate in less frequented airspace. The possible lack of passenger acceptance and inadequate legislation poses far greater challenges, as technological advances are developing exponentially in contrast to social, economic and regulatory frameworks [48].
In the following section, a sustainable product launch is presented and concrete solutions for emerging technological challenges are developed. Furthermore, safety measures for emergency scenarios are examined and the assimilation into the existing system is considered.

4.1 Gradual Phasing-In

Since the terms autonomy and automation are often mistakenly used synonymously, a clear demarcation is necessary. Automation describes the transfer of functions to machines, which in principle can also be performed by human beings. By contrast, an autonomous system in aeronautics is characterized by its ability to make independent decisions and thus to fly an entire mission without human intervention. As the success of MIRUS depends significantly on the market entry, it will be gradually phased in (see Figure 4.10). The transition from manned to unmanned flight operations is therefore more of an evolution than a revolution. At the present time, only 17 percent of respondents would take a pilotless aircraft [49]. For this reason, passenger transport initially takes place in Single-Pilot Operations (SPO). Under SPO, the Airline Operational Center Operator (AOCO), Ground Operator (GO) and Air Traffic Control Operator (ATCO) offer active support to the pilot in all flight phases. Furthermore, they also perform essential flight guidance and monitoring tasks in autonomous operations [50].

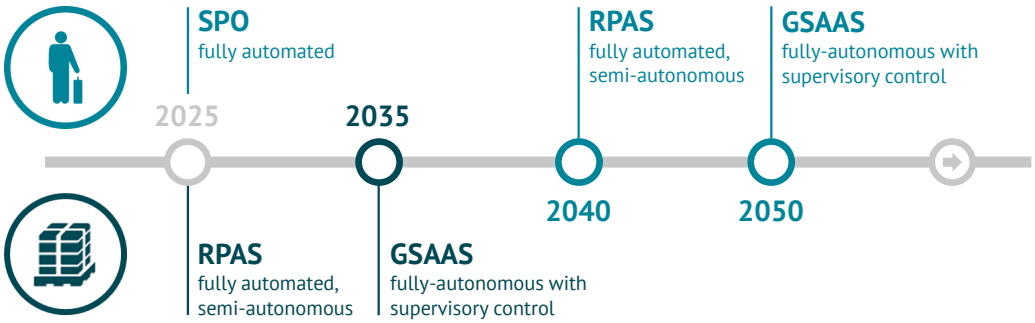

Figure 4.10: Road network to autonomy

The AOCO performs strategic tasks such as dispatch or route planning as well as coordination with the GO. The newly created GO authority assumes tactical tasks and is able to control and land the aircraft safely from the ground in case of an emergency. This cooperative decision-making and division of tasks additionally reduces the pilot's workload and thus the number of human errors. Aside from today's usual radio traffic, the communication between the various instances will increasingly take place via data link. Sufficiently reliable connectivity can be assumed due to a constant increase in the performance of the utilized systems [51].

In cargo transport, pilot status (human or autonomous) is not a limiting factor. For this reason, the implementation of a Remotely Piloted Aircraft System (RPAS) is initially introduced to cargo transport. Already in this phase, the intelligent autonomy system MIRI runs in a shadow mode. This enables the collection of essential flight data, which later simplifies decision-making in autonomous operations. In this operating mode, the aircraft is piloted by the GO. In the next step, the switch to autonomous cargo operations will take place (see Subsection 4.2), assuming that infrastructural and operational foundations as well as the regulatory framework for autonomous flight operations have been established. However, in this Ground Supervised Autonomous Aircraft System (GSAAS), the GO serves as a supervisory instance for multiple aircraft. The mission is defined as autonomous at the start of the taxi sequence. Increasing passenger acceptance is expected in the coming years due to a cross-sectoral trend towards autonomy. This will ultimately enable remote-controlled and, in the distant future, autonomous passenger operations.

4.2 Pre-Programmed Sequences

In autonomous flight operations, tasks to be performed manually by the pilot and decisions to be made must be taken over by appropriate systems. For this purpose, MIRI, which is based on artificial intelligence, and pre-programmed sequences are implemented. During RPAS operation, this system already supports the GO.
Tasks, which pilots have to perform manually, are nowadays defined in the Standard Operating Procedures (SOP). For autonomous operations, these routines are digitally stored and initiated by different trigger signals. These signals include external inputs (e.g. from the ramp agent), Air Traffic Control (ATC) clearances via data link or pre-programmed triggers from various aircraft systems (such as reaching an altitude or speed which implies the initialization of a particular action). Appendix D shows a generic depiction of the cascaded sequence run, which is explained by example in the following. The ATC clears the aircraft for take-off. This signal initiates the "Before take-off"-sequence. Within this sequence, all required actions are now performed according to SOP. As a first step, the cockpit crew will announce that the aircraft is about to take off. In autonomous operations, an acoustic message is automatically generated for the passengers in the cabin. In addition, the air conditioning system, for example, is switched on as required and the exterior lights are automatically activated. After successful execution of all pre-programmed actions, the "Before take-off"-sequence is considered completed and the follow-up "Take-off"-sequence is triggered. Thus, all sequences of the entire flight profile are processed consecutively.

4.3 Autonomous Environmental Perception and Recognition System

Due to the omission of the pilot, systems for the detection and recognition of the environment are necessary to ensure safe control of the aircraft. In the air, the ATC already provides sufficient aircraft separation. In order to avoid any possible approaches, MIRUS is equipped with a fully automatic TCAS system. If the aircraft is still on ground, e.g. during taxi operations, the view from the cockpit is the most important resource for ensuring accident-free taxiing at the airport [52]. Since there is no cockpit crew in the aircraft from GSAAS level on, this essential view of the pilot must be adequately replaced by technical installations. To make this possible, the Autonomous Environmental Perception and Recognition System (AEPRS) is implemented. The AEPRS ensures real-time imaging of the environment, using a wide variety of sensor technology. Comparing the data with stored databases enables the aircraft to recognize the detected objects. Based on Global Positioning System (GPS), systems such as the On-Board Airport Navigation System (OANS) already provide a detailed airport map showing the current aircraft position, to reduce the risk of erroneous taxiing manoeuvres. However, if there is a conflict between the external view and the OANS display, the pilot must intervene. For this purpose, an Enhanced Vision System (EVS) III from Gulfstream is part of the AEPRS. This system allows the pilot's entire field of view to be sensory monitored through the combined use of microwave radar and short-wave infrared radiation. Due to the specially tuned frequency, both the real-time detection of runway lights and the detection of runway markings, taxiways and obstacles are guaranteed with the help of this technology.

This optical recognition enables MIRUS to discern signs and markings at the airport and, by adjusting additional parameters, to initiate the corresponding sequences. As an example, the final runway holding position is visually detected by the appropriate marking. An additional positive comparison of the aircraft's GPS position with that of the last runway holding position enables the "Taxiing"-sequence to be completed and the "Before take-off"-sequence to be initiated. An Active Electronically Scanned Array (AESA) will be implemented to improve environmental perception in the air. Compared to conventional radar systems, this provides more flexible space scanning while simplifying maintenance and increasing reliability. If the collected data of the AESA are mapped with those of the EVS III, a fail-safe navigation is possible even in case of GPS problems.

4.4 Resilience Planning

In order to maintain the high safety standards, procedures and redundancies are implemented for both RPAS and autonomous operation. Three possible emergency cases are described below.
In case of a system failure in flight (see Figure 4.11), GO, AOCO and ATCO receive a corresponding message from the aircraft and are able to initiate pre-programmed emergency sequences. Since MIRI already runs in standby mode during RPAS operation, decisions made by the GO can be stored in the system. In emergencies on board (e.g. a heart attack) communication between passengers and the GO is ensured via a suitable interface (e.g. satellite telephone). Onboard cameras enable the GO to better assess the situation in order to take appropriate action. If the connection between the aircraft and GO/ATCO fails, reliable guidance or monitoring of the aircraft is no longer guaranteed. With the help of the implemented emergency autoland system, MIRI initiates the immediate approach of an alternate. A list of all alternative airports is stored in a database. This system is capable of independently searching for a suitable emergency landing area, guiding to the selected landing site and landing there safely [53]. In this case, it is the responsibility of the GO to inform all possible alternative airports about loss of control. Since MIRUS mainly serves smaller airports without ground-based facilities (such as the instrument landing system), this autoland system also enables safe landings at these airfields [54].

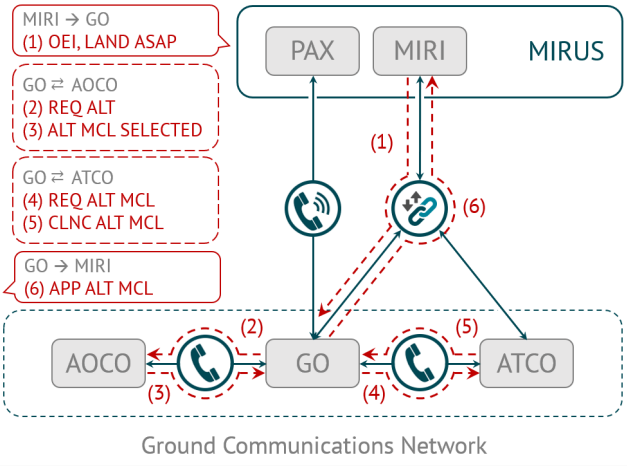

Figure 4.11: Communications network

4.5 Assimilation to Existing System

A highly performant system auch as MIRUS (especially in GSAAS mode) requires an adapted thought through overall air traffic system to deliver the ecological benefits and economical advantages it is capable of. Consequently, not only adjustments regarding autonomous flight operations have to be considered, but also challenges concerning ground handling. The routine walk as a mandatory pre-flight check of the pilot will be completely replaced by inspection drones (TRL 9) specially carried on board. Released as a time and cost saver in maintenance, this drone can reliable check the surface of the aircraft before each flight. By using more accurate and precise machines, precautions are also taken at the airport to minimize the human error and gradually eliminate it completely. By optimizing turnaround time management, increased punctuality can be assured and slots can be obeyed. In conclusion, enhancing the aircraft for independent handling as well as supporting GSEs further optimizes the ground handling process.

5 Aircraft Characteristics

This section gives a summary of the conceptual design of MIRUS. The goal is to generate a first coherent design of the aircraft by defining its dimensions and characteristics computationally.
As the maximum payload is independent from the range, there is no single but two design missions to be considered:

(A) The **Operational Range Mission** (120 NM, MTOM, 27 min) specifies the speed in cruise V_{CR} to maintain the flight time and thus the daily mission plan (see Subsection 2.2).

(B) The **Maximum Range Mission** (500 NM, MTOM, V_{CR}) determines the Maximum Take-Off Mass (MTOM) due to the maximum fuel mass necessary for this mission.

In the following, the design process of MIRUS is explained based on its computation algorithm.

5.1 Design Algorithm

The design algorithm for MIRUS is illustrated in Figure 5.12. The architecture with its iterative character consists of different design fields including various design modules. This allows multiple cases, such as the two design missions, to be considered simultaneously.

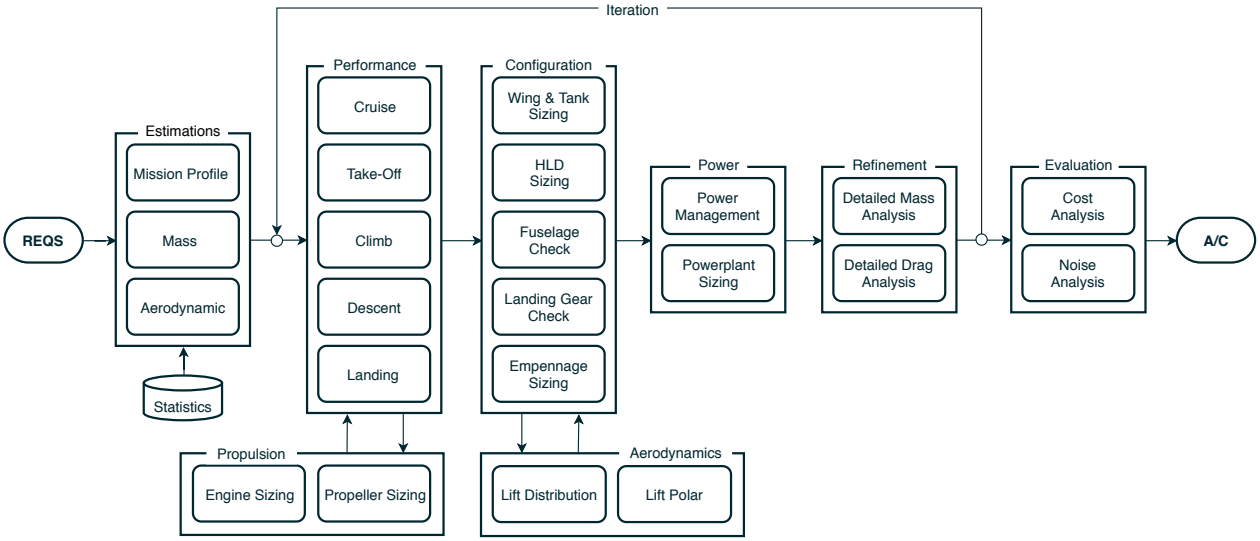

Figure 5.12: MIRUS' design algorithm

The conceptual design of an aircraft is always accompanied by a lack of data. Therefore, first estimations become mandatory beside the defined requirements. Those estimations are obtained from statistics or research and are used as input parameters for the iteration loop. Within the iteration loop, essential design fields, such as Propulsion, Configuration and Refinement, result in basic geometry and performance data. Hence, all input values are going to be corrected during the iteration. Finally, the converged solution is analyzed in terms of economic efficiency and noise emissions (see Section 6).

5.2 Performance

The aircraft performance capabilities are analyzed for all mission segments. Therefore, a Regular (REG) and a worst case mission scenario, which additionally covers all Alternate (ALT) and exceptional cases in-flight, are considered. Both profiles are collectively shown in Figure 5.13.
Each segment is characterized by different average performance parameters, which provide appropriate results regarding the conceptual design phase. In the following, all other performance parameters are determined for the regular flight mission. Alternates are proceeded analogously. Every performance calculation is carried out assuming International Standard Atmosphere (ISA) conditions for pressure, temperature and density.

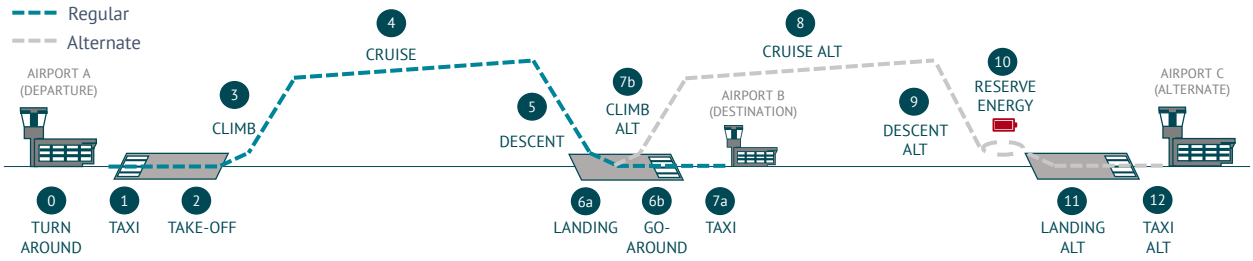

Figure 5.13: Mission profile

5.2.1 Take-Off

Any performance parameter during take-off is mainly driven by the Take-Off Field Length (TOFL), which is divided into two parts: first, ground roll path and second, initial climb to 35 ft path. For both paths a thrust to weight ratio T/W_{TO} is formulated, which derives from simplified equations of motion. Each ratio is modeled as a function of a variable ground roll coordinate $x_{\mathrm{TO,GND}}$, an initial climb to 35 ft coordinate $x_{\mathrm{TO,ICL}}$ and different performance parameters. In Figure 5.14 both functions are plotted for the Maximum Range Mission, as it defines the required thrust due to the corresponding maximum wing loading. Table 5.1 contains the relevant performance parameters. The scenario of a single engine failure during take-off is accounted for in accordance with the 14 CFR §23.2115. In order to set the engine failure recognition speed, the optimization concept of the Balanced-Field-Length is applied.

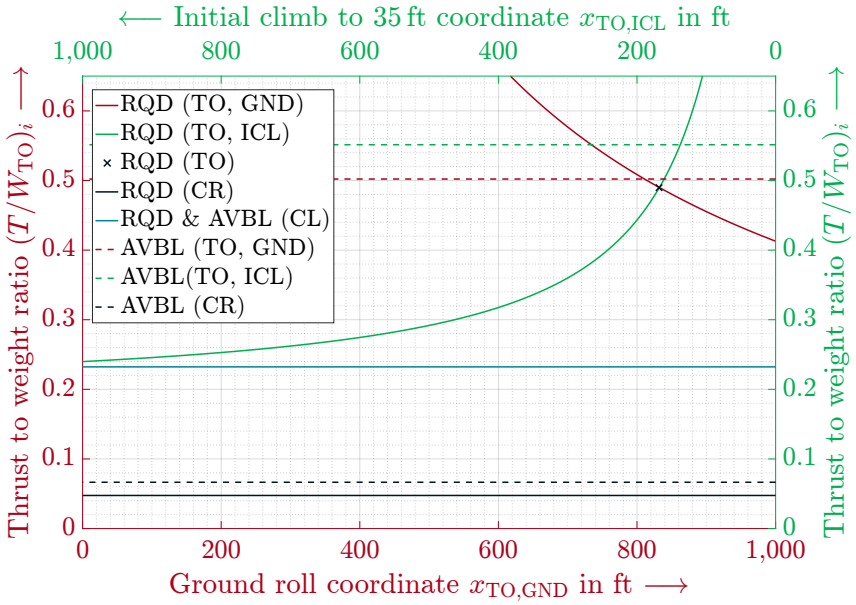

Figure 5.14: Thrust matching for Mission (B) at ISA MSL

Table 5.1: Take-off performance data for Mission (B)

Parameter	Value
TOFL	1,000 ft
T_{TO}	18.32 kN
$(T/W_{\mathrm{TO}})_{\mathrm{TO}}$	0.49
$(W/S)_{\mathrm{TO}}$	3,618 N/m²
$C_{L,\mathrm{TO}}$	3.75
$(C_L/C_D)_{\mathrm{TO}}$	8

In accordance with the CESTOL design philosophy, as mentioned in Subsection 3.1, the maximum wing loading of 3,618 N/m² is compensated by the actively generated lift coefficient $C_{L,\mathrm{TO}}$ of 3.75 in order to meet the short take-off length length.
By applying both coordinates in opposite directions, the required thrust for take-off (considering ISA MSL conditions) is matched. With a required thrust to weight ratio of 0.49, the take-off is decisive for the installed thrust. The available thrust, which is derived from Subsection 5.3, is even greater in order to proceed from aerodromes with higher elevation. The comparison of take-off, climb and cruise shows the huge spread between their thrust to weight ratios typical for STOL aircraft. Therefore, MIRUS is equipped with the third retractable propeller.

5.2.2 Climb

With regard to the climb segment, the Rate Of Climb (ROC) is the key performance parameter. It is necessary to climb as fast as possible in order to escape the horizontal speed limitation of 250 KIAS below 10,000 ft. Hence, enough time for cruise is left to keep the cruise speed at a moderate level. Therefore, the Operational Range Mission is considered for the climb performance. The optimum ROC or vertical speed w_{CL}, respectively, is determined by the Specific Excess Thrust (SET). Considering stationary climb, the SET γ_{E} is formulated in Equation (5.1).

$$\gamma_{\mathrm{E}} = \frac{T - D}{W} \qquad (5.1) \qquad D = C_D \cdot q \cdot S = \left(C_{D,0} + \frac{1}{\Lambda e \pi} \cdot C_L^2 \right) \cdot \frac{\rho}{2} V^2 \cdot S \qquad (5.2)$$

The thrust T equals the maximum available thrust under climb conditions, which is based on a thrust model mentioned in Subsection 5.3. In addition, a simple drag model, as formulated in Equation (5.2), is applied, which delivers sufficient results. The entire approach leads to a variable ROC depending on the corresponding speed. Figure 5.15 shows this relation for different altitudes. The optimum rates of climb are averaged and yield to a mean optimum ROC of 13.8 m/s. The corresponding performance parameters are listed in Table 5.2.

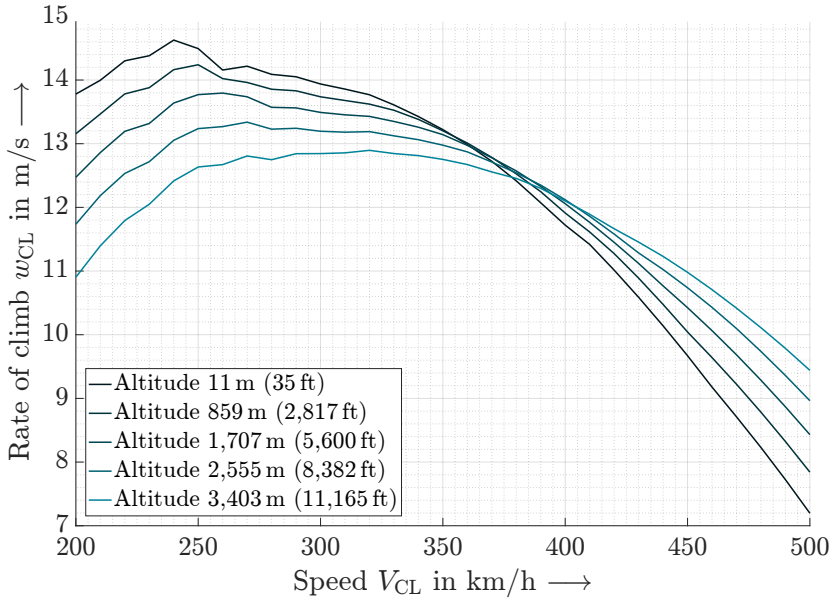

Figure 5.15: ROC for Mission (A)

Table 5.2: Climb performance data for Mission (A)

Parameter	Value
w_{CL}	13.8 m/s
V_{CL}	268 km/h
T_{CL}	8.66 kN
$(T/W_{\mathrm{TO}})_{\mathrm{CL}}$	0.23

5.2.3 Cruise

Performance target parameters for cruise are speed, altitude and thrust. The cruise speed can be determined according to the Operational Range Mission. By taking the total flight time and range into account, the cruise speed results from the other segments' parameters (turn-around is not included). This leads to a cruise speed of 618 km/h for all missions. Therefore, a constant Reynolds and Mach number and thus a constant available aerodynamic performance (as described in Subsection 5.4) is assumed. Since the lift coefficient $C_{L,\mathrm{CR}}$ and thus the drag to lift ratio $(C_D/C_L)_{\mathrm{CR}}$ would change due to loss of fuel mass, a continuous cruise climb is recommended to ensure constant required aerodynamic performance. Hence, two cruise altitudes must be taken into account: Initial Cruise Altitude (ICA) and Final Cruise Altitude (FCA). Both altitudes are determined assuming a stationary horizontal flight state, which is generally formulated in Equation (5.3).

$$C_L = W/S \cdot \frac{1}{\frac{\rho}{2} V^2} \qquad (5.3) \qquad T_{\mathrm{CR}} = W_{\mathrm{CR}} \cdot (C_D/C_L)_{\mathrm{CR}} \qquad (5.4)$$

The lift coefficient $C_{L,\mathrm{CR}}$ of 0.27 is determined considering the constant cruise speed V_{CR}, atmospheric conditions on the minimum initial cruise altitude of 10,000 ft (see Subsection 2.1) and the highest wing loading $(W/S)_{\mathrm{CR}}$ according to the Maximum Range Mission. Hence, any other mission has a higher ICA than 10,000 ft, as it must have a lower wing loading. The FCA depends on the reduction in the wing loading during cruise. By solving Equation (5.3) for ρ, the FCA can be determined. The required cruise thrust results from an adjusted equilibrium of forces showed in Equation (5.4) combined with the drag model mentioned in Equation (5.2). All cruise performance parameters are listed in Table 5.3.

Table 5.3: Cruise performance data

Parameter		Value Mission (A)		Value Mission (B)	
V_{CR}	($\hat{=}M_{\mathrm{CR}}$)	618 km/h	(0.53)	618 km/h	(0.53)
ICA		3,403 m	(~11,165 ft)	3,048 m	(~10,000 ft)
FCA		3,483 m	(~11,427 ft)	3,458 m	(~11,345 ft)
T_{CR}	($\hat{=}(T/W_{\mathrm{TO}})_{\mathrm{CR}}$)	1.74 kN	(0.0482)	1.78 kN	(0.0476)
$C_{L,\mathrm{CR}}$		0.27		0.27	
$(C_L/C_D)_{\mathrm{CR}}$		20.6		20.6	

5.2.4 Descent

A fast descent benefits the cruise speed, similar to the climb. The descent is assumed to be a glide flight, which yields to the Rate Of Descent (ROD) being a function of speed and altitude (visualized in Figure 5.16). The mean descent performance parameters are given in Table 5.4. By changing the speed V_{DS} within the following phases the flight path is defined:

Phase 1: Decelerating from cruise speed to 95 percent of 250 KIAS (above FL100)

Phase 2: Keeping 95 percent of 250 KIAS constant

Phase 3: Decelerating to safety speed until 35 ft

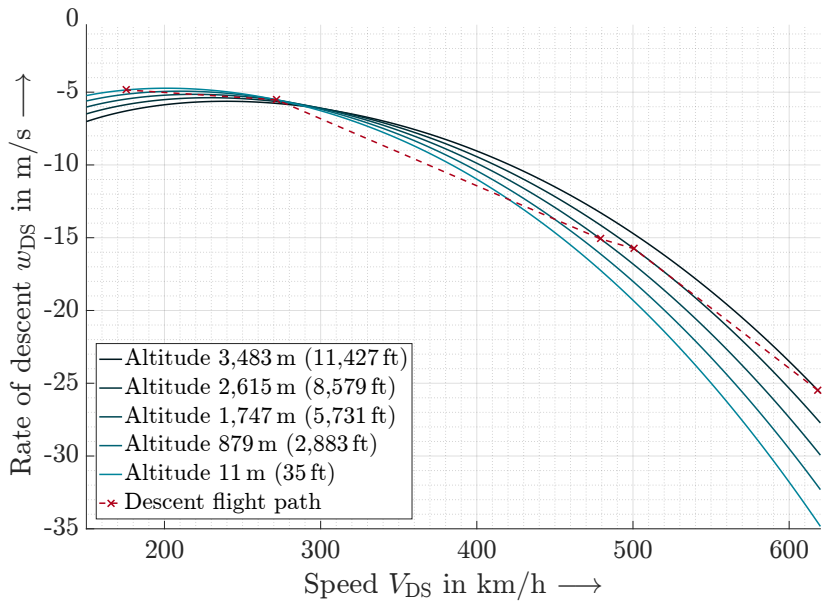

Figure 5.16: ROD for Mission (A)

Table 5.4: Descent performance data for Mission (A)

Parameter	Value
w_{DS}	−13.3 m/s
V_{DS}	409 km/h
γ_{DS}	−6.3 °

Table 5.5: Landing performance data for Mission (B)

Parameter	Value
LFL	1,000 ft
γ_{app}	−5 °
V_{app}	176 km/h
$(\mathrm{W/S})_{\mathrm{LDG}}$	3,460 N/m²
$C_{L,\mathrm{LDG}}$	4
$(\mathrm{C_L/C_D})_{\mathrm{LDG}}$	5

5.2.5 Landing

In essence, the landing performance is defined by the Landing Field Length (LFL). It limits the maximum landing wing loading, which can be derived from a balance of energy for the landing approach. This approach is also divided into two phases similar to the take-off procedure. The resulting relevant performance data for landing can be found in Table 5.5. As the landing requires the highest lift coefficient of 4, it defines the maximum power of the high-lift devices.

5.3 Propulsion System

All three propulsion units are assumed to be equal in their performance. In the following, both components - the propeller and the electric engine - will be configured based on the effect chain in Figure 5.17.

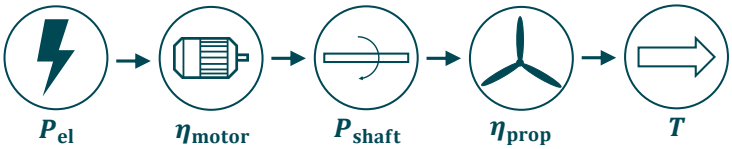

Figure 5.17: Effect chain of the propulsion system

5.3.1 Engine Sizing

The electric engine is considered to be a black box, which receives electric power P_{el} as an input and provides mechanical power P_{shaft} as an output. Therefore, a relation between both power quantities in terms of an efficiency factor η_{motor} is required. As the mechanical power and the efficiency factor are a function of the motor speed or Revolutions Per Minute (RPM), respectively, a model is needed, which contains the relation of all four parameters. Therefore, the electric motor is modelled after existing motors. The basis are the power to motor speed relation and the efficiency chart of an EMRAX 348 derived form its data sheet [55]. Additionally, technology factors are applied on torque and motor speed derived from the electric motor SP260D developed by Siemens [56]. This results in the motor performance parameters shown in Table 5.6.

5.3.2 Propeller Sizing

The propeller design is carried out with the Generalized Method of Propeller Performance Estimation from Hamilton Standard. This method is based on different performance maps, which define the propeller performance for a specific propeller geometric configuration considering all potential operating conditions [57]. In the first place, the propeller diameter needs to be specified. The diameter is designed for an efficient cruise as this segment of Mission (A) takes 62 percent of the whole flight time. Therefore, the required electric power $P_{el,CR}$ is analyzed with regard to a varying diameter D_{prop} based on Equation (5.5) and visualized in Figure 5.18. However, the maximum diameter is limited due to the blade tip mach number while running on peak motor speed.

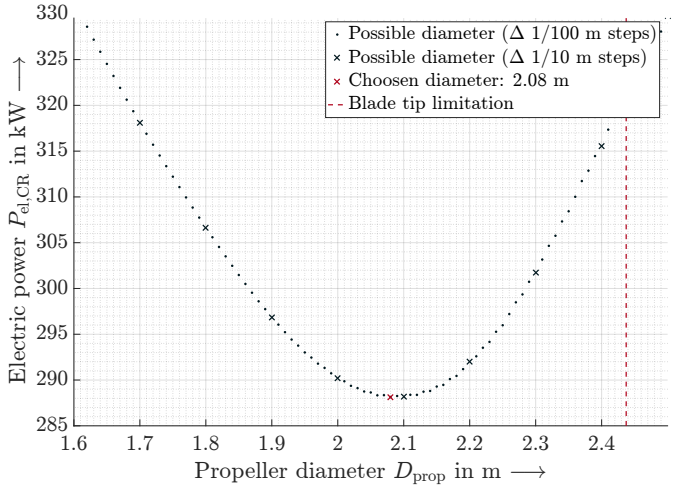

Figure 5.18: Propeller diameter sizing

Table 5.6: Electric engine parameters

Parameter	Peak	Continuous
RPM	2,520 $^{1}/_{min}$	2,520 $^{1}/_{min}$
P	485 kW	233 kW
P/m	9.7 $^{kW}/_{kg}$	4.66 $^{kW}/_{kg}$

$$P_{el,CR} = \frac{T_{CR} \cdot V_{CR}}{\eta_{motor} \cdot \eta_{prop}} \qquad (5.5)$$

$$\text{with } \eta_{prop} = f(D_{prop})$$

As a small diameter turns out to be inefficient it requires much more power to generate the needed thrust. Any diameter, which is too large, causes blade tip losses and thus a higher power demand. The optimum diameter is characterized by the minimum required power and equals 2.08 m. With the diameter set, the available thrust and power for take-off, climb and cruise can be determined by using the Hamilton Standard method analogously.

5.4 Configurational Sizing

All basic components are dimensioned in the configurational sizing. As the fuselages dimensions derive from the cabin design and system positioning (see Subsection 3), it is not further discussed. The same applies to the gear, which, in the scope of the conceptual design, is only configured in order to comply with the clearance angle to the side ($> 7\,^\circ$) and to the rear ($> 10\,^\circ$).

5.4.1 Wing Sizing

The wing is designed with regards to define the planform, airfoil, tank and aerodynamic parameters. Its planform (illustrated in Figure 5.19) is defined by the wing area S_W, which derives from the wing loading and mass. Further geometric constraints are set in Table 5.7, such as aspect ratio Λ_W, taper ratio λ_W and sweep $\varphi_{\mathrm{W},25}$. A high aspect ratio of 12 and therefore a high wing span b_W of 11.1 m is chosen to minimize the induced drag. The laminar airfoil NACA 65-210, with a maximum thickness at 40 percent of the chord, is used for the wing due to its relatively high maximum lift coefficient. Considering the Maximum Range Mission, the usable volume of the tank is specified, which is limited by the front and rear spar. Correction factors are applied, since the volume is affected by structure like ribs and changing temperatures. By using a modified semi-empirical lift coefficient distribution method (according to Diederich), the available aerodynamic performance of the wing is analyzed [58]. As illustrated in Equation (5.6), the original method is based on a dimensionless circulation γ that can be divided into a circulation depending on the planform geometry γ_a and one depending on the wing twist γ_b. The modified version enables the integration of the High-Lift Devices (HLD) into the lift coefficient distribution by adding a further circulation γ_c. Therefore, γ_c is determined analogously to γ_b. Instead of a real wing twist, an equivalent Angle Of Attack (AOA) in the span-wise region of the HLD is used. This AOA derives from the airfoil lift gradient and the maximum lift coefficient generated by the HLD. As a result, the lift coefficient distribution and the corresponding available lift coefficient of the wing are determined.

$$\gamma = \underbrace{\underbrace{\gamma_\mathrm{a} \cdot C_{L,\mathrm{W}} + \gamma_\mathrm{b}}_{\text{Original Diederich}} + \gamma_\mathrm{c}}_{\text{Modified Diederich}} \tag{5.6}$$

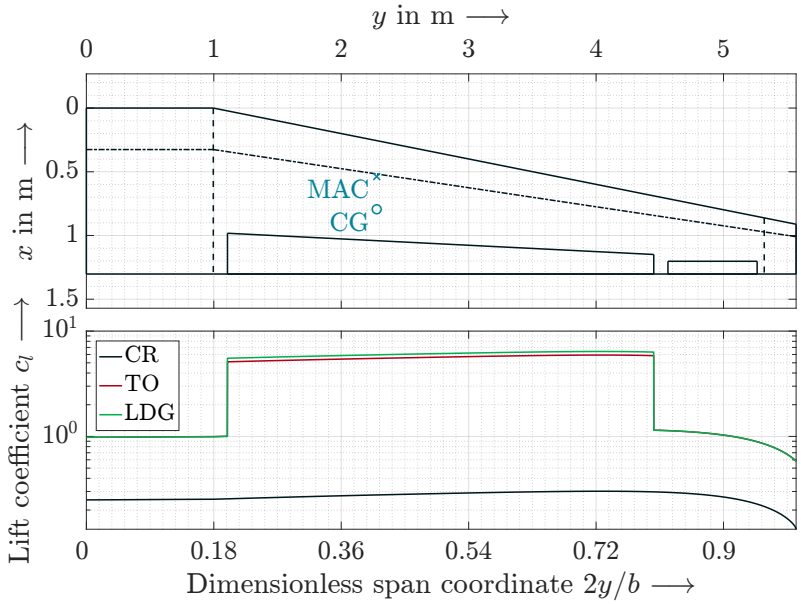

Figure 5.19: Wing planform and lift coefficient distribution

Table 5.7: Wing parameters

Parameter	Value
Geometric parameters	
S_W	$10.3\,\mathrm{m}^2$
Λ_W	12
b_W	11.1 m
λ_W	0.3
$\varphi_{\mathrm{W},25}$	$7.7\,^\circ$
$\varepsilon_{\mathrm{W,root}}$	$2.7\,^\circ$
Aerodynamic parameters	
$C_{L,\mathrm{W,CR}}$	0.27
$C_{L,\mathrm{W,TO}}$	3.8
$C_{L,\mathrm{W,LDG}}$	4.07

5.4.2 High-Lift Devices

The purpose of HLD is to provide additional lift augmentation. Depending on the flap chord, flap deflection and blowing coefficient, an additional lift coefficient is determined for the airfoil lift polar (Equation (5.7)). In order to inject additional momentum in the boundary layer, the jet velocity has to be greater than free stream velocity. The benefit of active flow control in aerodynamic lift is

represented by the Lift-Gain-Factor (LGF) (Equation (5.8)). Previous numerical and experimental investigations show that LGF values of around 80 are achievable [59] [60]. The necessary compressor power is a function of pressure ratio and mass flow rate, which depends on jet velocity and slot area. For both, experimental and numerical investigations imply that there is an optimum of approximately four times the free stream velocity and 0.06 percent of chord length for slot height (see Table 5.8). The desired mass flow rates and pressure ratios imply the choice of single staged axial compressors, for which the mechanical power can be determined by Equation (5.9), where the total temperature at the compressor outlet is dependent of compressor pressure ratio. The compressor system mass (including electric motors, compressors, cables, generators, gearboxes and converters) is determined by linear regression depending on the mechanical output power. With advanced materials, a resulting specific mass is calculated with Equation (5.10) [61].

Table 5.8: CCW parameters

Parameter	Value
$h_{\text{slot}}/c_{\text{wing}}(y)$	0.06 %
$c_{\text{flap}}/c_{\text{wing}}(y)$	25 %
P_{CMP}	60 kW
Π_{CMP}	2
$\dot{m}_{\text{jet}}$	0.98 kg/s

$$C_\mu = \frac{\dot{m}_{\text{jet}} \cdot V_{\text{jet}}}{\frac{\rho_\infty}{2} \cdot V_\infty \cdot S_{\text{ref}}} \tag{5.7}$$

$$\text{LGF} = \frac{C_{L,\max} - C_{L,\text{ref}}}{c_\mu} \tag{5.8}$$

$$P_{\text{CMP}} = \dot{m}_{\text{jet}} \cdot c_p \cdot (T_{\text{tot,CMP,out}} - T_{\text{tot,CMP,in}}) \tag{5.9}$$

$$m_{\text{CCW}} = 0.485\,\text{kg/kW} \cdot P_{\text{mec}} + 196.95\,\text{kg} \tag{5.10}$$

The use of high velocity jet actuation can be divided into two flow phenomena, depending on the jet momentum coefficient. In the first regime, called boundary layer control, the Coanda effect forces the flow to the surface until it is fully attached and no separation occurs. By increasing the jet momentum even more, the second regime of circulation control is reached, where the jet generates an extended circulation aft the flap downstream increasing the circulation further. Ensuring maximum efficiency, the compressors are designed to provide enough momentum forcing an attachment of the flow over the whole flap at maximum desired deflection angle [59].
The manipulation of circulation at the trailing edge affects the flow around the whole airfoil, creating a dominant suction peak at the leading edge. To prevent leading edge separation and increase the maximum angle of attack, the leading edge consists of a flexible droop nose. This is capable of morphing the shape by changing its angle and radius without any discontinuities or obstacles [62].

5.4.3 Empennage

The main design drivers for the Vertical Tail (VT) are the single engine failure scenario and the crosswind landing capabilities. In the first case, the vertical stabilizer must be able to counter the yaw moment in case of wingtip engine failure at minimum control speed according to 14 CFR §23.149. For the second case, 14 CFR §25.237 demands to counter a crosswind component of at least 20 kts. A bank angle of 5 ° is allowed for the following calculations.
By varying aspect, taper and area ratios, the related vertical tail derivatives are calculated [63] [64]. A moderate sweep is applied in order to maximize the lever arm for both the horizontal and vertical tail. However, the aft mounted propeller limits the maximum sweep. In order to reduce drag and save mass, the vertical tail with the smallest surface and lowest aspect ratio is determined (see Table 5.9). The Horizontal Tail (HT) sizing is done for both the horizontal stabilizer and the forward canard wing (CW). For a given CG range, controllability and static stability must be ensured by the control surfaces. Therefore, the stability and control diagram is created (see Figure 5.20). As can be seen, for all CG positions controllability and static stability is given with the minimum possible control surface area. Furthermore, the required maximum landing lift coefficient must be maintained. The related aerodynamic characteristics are calculated similar to the vertical tail sizing. The canard wing receives a high taper ratio of 0.9 in order to prevent tip stall due to low local Reynolds numbers. Additionally, conventional high-lift devices are installed in order to guarantee controllability at front CG position.

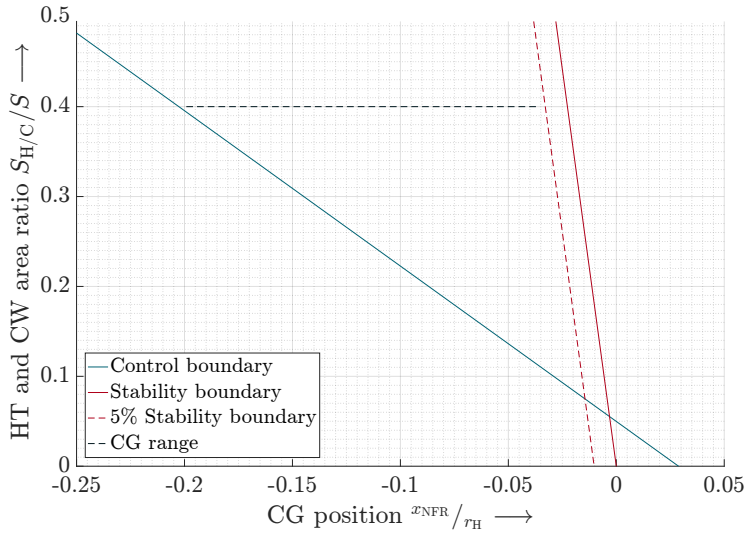

Figure 5.20: Stability and control diagram

Table 5.9: Empennage data

Parameter	VT	HT	CW
Λ_i	1.75	6	6.5
λ_i	0.63	0.6	0.9
S_i/S_W	0.4	0.24	0.16
$\varphi_{25,i}$	14.9 °	30 °	0 °

5.5 Powerplant Sizing

The hybridization of the powerplant system is based on the required power and energy during each segment. In essence, there are three consumers, which are determined using three different approaches. According to Equation (5.5), the propulsional power is calculated, whereas the power of the active high-lift devices derives from the compressor performance as mentioned in the previous subsection. All non-propulsion components, such as avionics and cabin electronics, are also considered in the power determination by using a linear approach. Thereby, a basic and a variable power need is taken into account. Hence, the total required energy results from power multiplied by time.

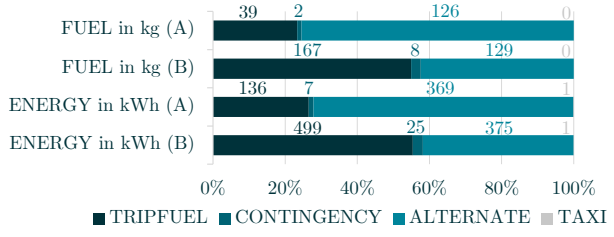

Figure 5.21: Energy and fuel mass breakdown for Mission (A)/(B)

Table 5.10: Powerplant data for Mission (B)

Parameter	BAT	CAP	GEN
$(P/m)_i$ in W/kg	1,300	5,000	2,812
$(E/m)_i$ in Wh/kg	176.5	15	-
$P_{max,i}$ in kW	326	745	319
$E_{max,i}$ in kWh	44.22	2.24	-

The hybridization is defined by distributing the required power and energy to the Battery (BAT), supercapacitor and Generator (GEN). Therefore, the following criteria are specified:

- The generator is designed for cruise power as this segment is characterized by a high energy amount at a relatively low power level. Defining a constant Specific Fuel Consumption (SFC) of $\dot{m}_F/E_{GEN} = 0.35\,\mathrm{kg/kWh}$, the generator is considered to run stationary from take-off to landing.
- The climb segment defines the necessary power of the lithium-ion battery while it is supported by the generator. It is intended to find a compromise between lifetime and capacity utilization. Therefore, the batteries are limited in their State Of Charge (SOC) within a range of 30 to 80 percent and in their charging rate of approx. 1 C. Hence, a total number of cycles from 5,200 to 6,800 are expected [65]. In order to save battery mass, the total energy capacity of the accumulators is kept as low as possible. Thus, the battery is recharged during the energy-efficient descent to cover the following segments' needs.
- The CAP is the main power supplier during the short take-off as it discharges quickly and provides an extraordinarily high power. Mass savings are achieved similarly to the battery, except for the capacity limitation, since this is not critical for the CAP's lifetime.

Figure 5.21 shows a breakdown of the energy and fuel consumption. The block energy on board is E_{block} for Mission (A) is 513 kWh and for Mission (B) is 900 kWh (see Table 5.10). The required block fuel mass for both missions amounts 167 kg and 304 kg. Additionally, a more detailed description of the powerplant hybridization is given in Appendix E including an overview of the SOC and energy consumption for each mission segment. The consumption does not include the contingency.
Accumulators and capacitors are characterized by their co-related specific power P/m and specific energy E/m, which are derived from a Ragone plot [66]. Based on these specific parameters and the given hybridization, the powerplant components' masses are determined. To ensure sufficient redundancy, a factor of 1.2 is additionally applied, which results in a battery mass of 301 kg and a capacitor mass of 179 kg. The gas generator's mass of 113 kg is determined by a statistic regression. Its fuel consumption is determined considering the SFC and energy generation of each segment.

5.6 Lighter by Design

An accurate mass prediction at the conceptual design stage is essential for a proper calculation of the maximum take-off mass. Therefore, two semi-empiric mass prediction methods according to Raymer and Nicolai are used, which turn out to be suitable for the mass determination [67] [31]. As MIRUS is equipped with unconventional systems, not all masses are derived from these methods. The propulsion system is divided into smaller system groups. For this purpose, the propeller mass is determined by the Hamilton Standard method and the engine mass by values from research. A surcharge factor is taken into account for additional components. As extremely high three-phase alternating currents flow between powerplant and propulsion system, correspondingly sufficient aluminum cables must be implemented. Among other, the cross-sectional area is dependent on the electric current and the cable length [68]. With a resulting area of 336 mm^2 and a corresponding diameter of 19.5 mm the cable mass amounts 91 kg. Powerplant and HLD masses can be found in the respective subsection. The basic masses are summarized in Table 5.11 and Figure 5.22. A detailed mass breakdown is included in Appendix F. The MTOM of 3,815 kg is defined by Mission (B) and the PAX-layout. Due to its modular cabin design with seats mounted on pallets more mass has to be taken into account compared to the cargo layout. MIRUS proves to be slightly lighter than potential reference aircraft such as a Piaggio P-180, Eviation Alice, Beechcraft Starship and ZUNUM ZA10. Among other factors, the short range is the main driver for these mass differences. Positioning all components and considering all possible CG positions, the CG range can be determined.

Table 5.11: Basic mass breakdown for PAX version

Parameter	Mission (A)	Mission (B)
OEM	2,613 kg	2,613 kg
ZFM	3,511 kg	3,511 kg
Fuel	167 kg	304 kg
MTOM	3.678 kg	3,815 kg

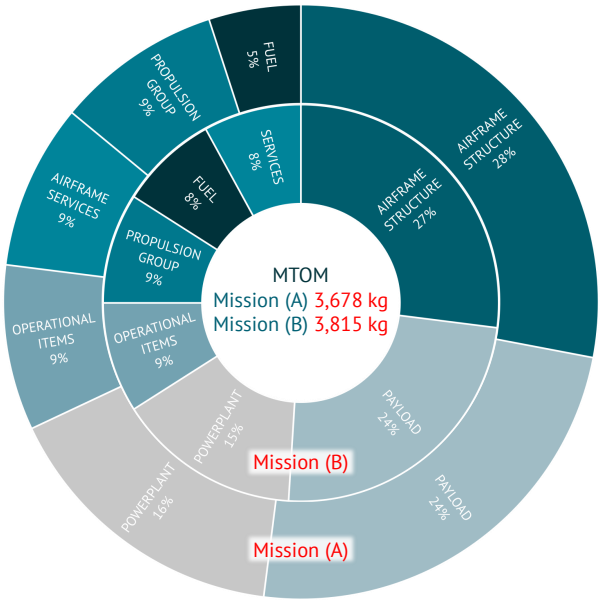

Figure 5.22: Mass breakdown for Mission (A)/(B)

6 Optimization to the Core

In addition to performance features, a holistic aircraft design is characterized by a balanced consideration of economic and ecological aspects. In the following, the design is therefore examined with regard to noise emissions, operating costs and the achievement of the top level aircraft requirements.

6.1 Noise

In order to comply with 14 CFR §36, Appendix G, a numerical noise simulation is used. The A-weighted Sound Pressure Level (SPL) at the Measurement Point (MP) is calculated, resulting from the aircraft's movement along the method's defined path. Note that 14 CFR §36, Appendix G requires the usage of take-off power setting in the initial climb segment, unless „[...] airworthiness limitations do not allow the application of take-off power and RPM up to the reference point". This is the case since MIRUS' CAP run out of charge before reaching the measurement point. According to the procedure, the maximum continuous power setting is applied during the initial climb, which is demonstrated in Figure 6.23. Using NASA's Aircraft Noise Prediction Program (ANOPP) method, the effective pressure in the various third-octave bands at the measurement point is calculated as the aircraft moves along the flight path [69]. Table 6.12 contains information about the modelled individual noise sources, the corresponding method used and their contribution to total SPL. Note that flaps and landing gear make no contribution to peak noise at the measurement point since they are retracted when passing over it. However, these noise sources are used in the noise contour map. Gas turbine related noise is not considered, assuming its position inside the fuselage grants sufficient acoustic shielding against high frequency turbine noise. Furthermore, the jet exhaust is not used for thrust generation, eliminating another noise source of turbine engines [69].

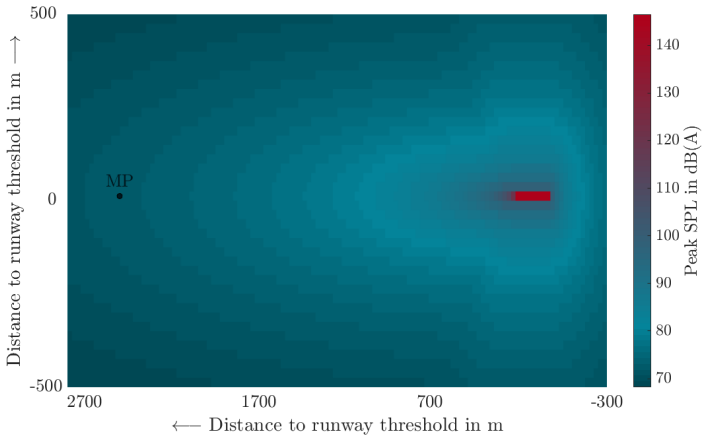

Figure 6.23: Peak noise contours during take-off

Table 6.12: Simulated A/C noise (MP)

Source	Method	SPL
Wing	ANOPP	52 dB(A)
Flaps	ANOPP	$-\infty$ dB(A)
Gear	ANOPP	$-\infty$ dB(A)
Propellers	Empirical	72 dB(A)
Motors	Empirical	54 dB(A)
Total		**73 dB(A)**

For the propellers and electric motors, each SPL is estimated using empirical formulas [69] [70]. Due to the high rotational speed of the propellers during take-off and climb, no significant propeller noise reduction can be expected from using electric motors [71]. Since propeller noise is dominating, actions to reduce certification noise levels must focus on the rotors. Potential technologies are swept blade tips (TRL 8), which reduce noise levels around three to four dB(A) [72]. With this modification, MIRUS achieves a total noise level of 73 dB(A).

6.2 DOC

To prove that MIRUS is a competitive product, the estimation of developing and operating costs is the major evaluation criterion. Most cost analysis methods are based on a statistical approach. Due to experience gaps, it may be a challenge to implement the effects of new technologies (e.g. CCW and hybrid-electric system). Most well-known methods focus on the operation of airliners and have to be adjusted for the use of commuter aircraft. Additionally, inflation needs to be considered - especially when using older methods. For this reason, all prices are adjusted to the consumer price

index of 2018. For the determination of the development costs, Gudmundsson provides a version of the DAPCA-IV method by RAND Corporation that has been modified by Eastlake for general aviation and business aircraft [73] [74]. Within this method, development costs are estimated based on the expected weight of the bare airframe and maximum level airspeed. Taking more complex technologies into account, such as composites used in primary or secondary structures, complex flap systems and pressurization, correction factors are applied [29]. Since costs for the hybrid-electric powertrain are not covered by this method, the calculation of these components is done by adding the individual list price. Furthermore, a quantity discount factor is introduced for parts where the value depends on the quantity purchased. The prices of the battery and supercapacitor are tied to their total capacity. Therefore, prices of 172 $/kWh and 2,400 $/kWh are assumed [75] [76]. The material cost of the necessary wiring is estimated with $8 per meter. The fractions of cost per unit are shown in Figure 6.24.

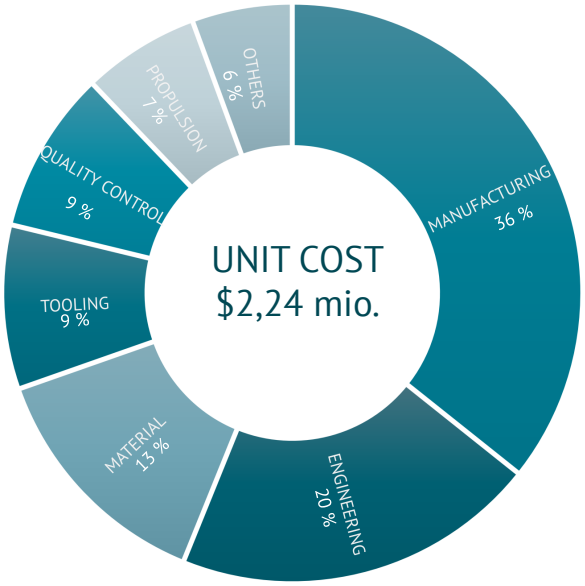

Figure 6.24: Unit cost of MIRUS

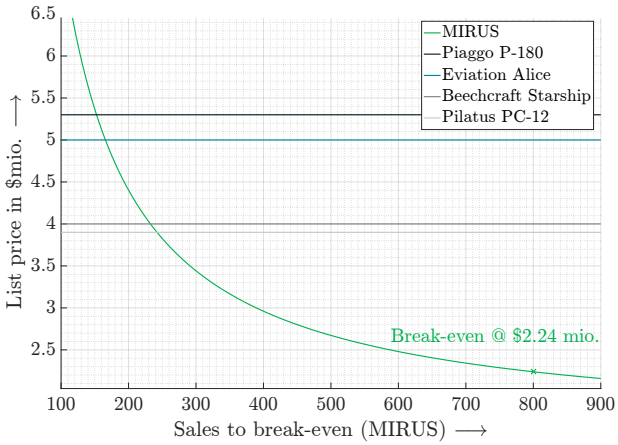

Figure 6.25: Break-even analysis

A break-even point analysis is used to determine the number of units needed to cover total costs. The costs per unit depend on the number of units sold (see Figure 6.25). A minimum list price of $2.24 million is obtained assuming that 800 aircraft will be sold. Compared to the list price of similar aircraft, the minimum list price of MIRUS is far below. Considering an additional profit margin, MIRUS still promises to be price competitive.
Not only development costs but also Direct Operating Costs (DOC) are investigated by using a method of the Association of European Airlines for Short and Medium Range Aircraft [77]. Similar to development costs, individual cost items are replaced by more suitable calculation approaches. The maintenance costs are estimated using the method provided by Gudmundsson, whereas the fuel and energy costs are calculated based on the estimated fuel mass and energy consumption from Subsection 5.5 [29]. Further adjustments are made in terms of ground handling fees to account for the retractable stairs and the capability of an independently push-back [78]. In order to ensure proper comparability, the DOC are related to the seat miles offered. The resulting Seat Mile Costs (SMC), defined as the DOC per PAX and mile, are shown in Figure 6.26. Another DOC related parameter are the Block-Hour Costs (BHC), which are compared to existing cost data for aircraft under operating rule 14 CFR §135 provided by the Federal Aviation Administration (see Table 6.13) [79]. Further reductions in operating costs are possible as soon as the regulations allow autonomous flight operations. Saving the crew costs would reduce SMC by 6.3 cent. It is likely that these savings will be offset by an increase in navigational fees, however, it is not possible to estimate an exact value due to unknown future regulations.

Table 6.13: Comparison of block-hour costs

Aircraft type	BHC	Difference
MIRUS	$345	-
MIRUS (autonomous)	$285	-$60 (-17%)
Turboprop airplanes (1-9 seats, one-engine)	$751	+$406 (+118%)
Turboprop airplanes (1-9 seats, multi-engine)	$1,726	+$1,381 (+400%)

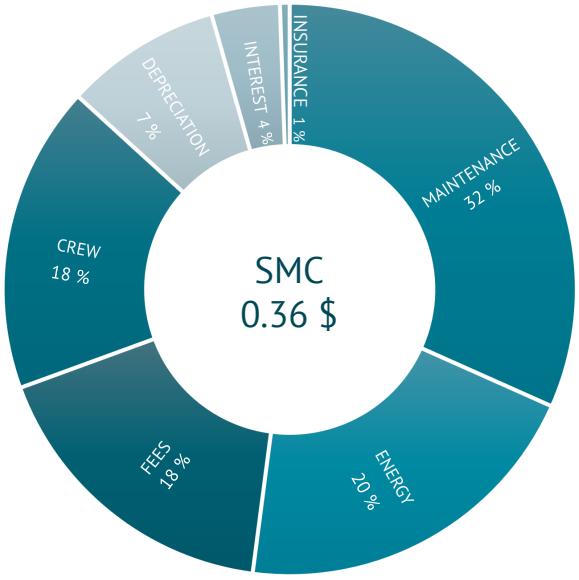

Figure 6.26: Direct operating costs per seat mile

6.3 Degree of Compliance

MIRUS, which is optimized to the core, completely fulfills all requirements defined in Section 2. Figure 6.27 shows the degree of compliance regarding the essential design criteria. It should be noted that all design criteria not shown in the overview have achieved the goal. The defined maximum range of 500 NM is performed within a block time of 95 minutes. This results in a mean block speed of 585 km/h, which is 91 km/h faster than the one of the operational range mission. This is due to the significantly longer cruise segment, which is proceeded at the same cruise speed and thus dominates the other mission segments to a greater extent.

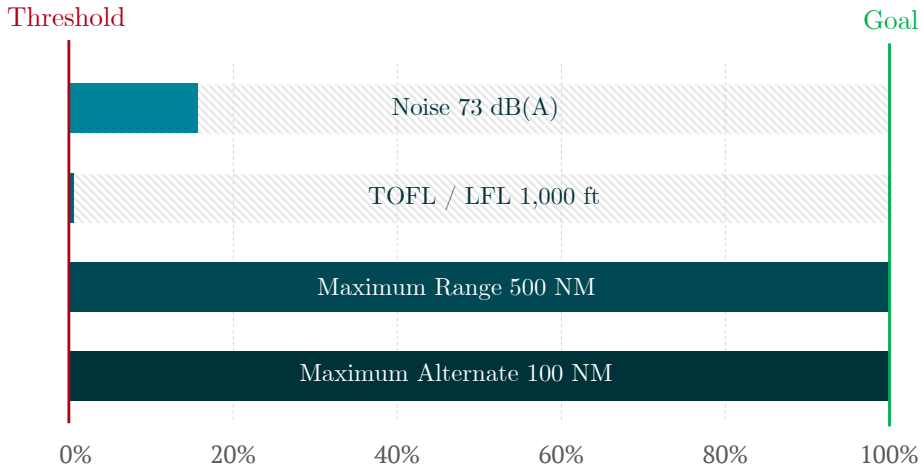

Figure 6.27: Compliance check

The TOFL and LFL of 1,000 ft results in MIRUS being equipped with an extraordinary high-lift system. Since the field length of most airports is significantly longer, this requirement seems oversized today. However, such a requirement is more reasonable for future infrastructure needs.
With regard to the noise requirement, a trade-off had to be conducted between noise and efficiency. The requirement of 65 dB(A) could not be met in favour of lower energy consumption and thus a cost-reducing design with a total SMC of $ 0.36. In Appendix G a technical data sheet is provided.

7 Conclusion

In the coming decades growing pressure on emerging markets transport systems will be exacerbated by rapid growing population and hence rising urbanization. At the same time, many areas of the USA face inadequate infrastructural connectivity resulting in social isolation and hopeless future prospects. These prevailing market trends clearly indicate a strong need for efficient commuter aircraft in both emerging and mature markets. Key to a sustainable transport development is an ambitious commuter program that, on one hand, aims to reduce congestion by giving people the possibility to live in rural areas while working in the city and, on the other hand, boosts the connection of rural areas to the amenities of civilization. As an integral part of future mobility concepts, small commuter aircraft form a growing market sector that neither can be served economically by other types of aircraft nor can be addressed by other means of transport. Thus, to establish their position over the long-term, they have to provide an enormous route flexibility and peerless operational versatility.

Focussing on the discussed future demands, this design study established the unique, versatile concept of MIRUS (fully compliant to 14 CFR §23, §135), leading into new commuter era. It shows the first conceptual design of a hybrid-electric driven, three surface aircraft with its synergistically integrated system: the circulation control wing. A main objective of the present design is the development of a CESTOL characteristic, which is achieved by combining an innovative three surface configuration with circulation control wing and a third retractable propeller providing extra power for take-off. It is the serial hybrid system that enables the use of electric motors, which, due to their low weight, allow the positioning of the engines at the wingtips. This results in an extraordinary, aerodynamically enhanced configuration. Exceptional efficiency is achieved not only by the powerplant but also by the use of an electrically driven wheel hub motor, enabling to operate independently from ground service facilities. The unprecedented modular cabin concept is paving the way towards an individually customizable cabin layout to guarantee the best passenger experience and most efficient cargo transport. This astonishing modular architecture offers unlimited flexibility in cockpit design, allowing a seamless transition from manned to unmanned flight operations. Offering a level of autonomy, where systems exhibit operational behaviour indistinguishable from that of a human pilot, MIRUS is not only meeting but also exceeding todays' safety requirements. Using the most advanced technology, MIRUS supports low-emission, lasting development in accordance with the Sustainable Development Goals. The present design is auspicious in every way, as all requirements are fulfilled and the overall target function, minimum operating costs, is achieved. With seat mile costs of $ 0.36, MIRUS is highly cost-effective and a key factor in establishing an affordable commuter service around the world.

Challenges that need to be addressed are the integration into the future air traffic system and possible modifications at airports served. For example, it would be advantageous to have a widespread supply of high voltage electricity at the airports.

The passenger acceptance could develop in both directions. Some are looking forward to an innovative, evolutionary air transport system. However, others might reject the windowless design or consider pilotless operations to be too dangerous. Especially regulations, for instance concerning the certification process, need to be adapted in order to operate autonomous aircraft.

Due to the imminent entry into service and the servicing of smaller, remote airfields, the transition to alternative fuels is initially not feasible. On account of their low power to weight ratio, fuel cells are not used in favour of a gas turbine. Assuming steady technological progress, the conversion to a non-fossil fuel, such as hydrogen, will be worthwhile in the future.

Finally, more detailed concept studies are necessary in order to reach the next design stage. However, MIRUS is right on track to face the challenge of boosting the neglected segment of commuter aircraft and stands by its statement:

Marvelous. In Every Way.

Appendix

Appendix A Technology Readiness Assessment

In the following table the key technologies used in the MIRUS design are listed and evaluated regarding their current development status.

Table A.1: List of key technologies

Group indication	Concept	Description	TRL
Aircraft Configuration	Three Surface Configuration	Proven configuration, used on Piaggo P.180 [80].	9
	Wingtip Mounted Engine	Used in combination with low aspect ratio wings for VTOL/STOL purposes (e.g. Bell-V22 Osprey) [81].	9
Aerodynamics	Circulation Control Wing	Successfully tested on a converted Grumman A-9 carrier jet [82].	8
Structural	Composite Structures	Common materials used in the development of new aircraft (e.g. Airbus A350) [83].	9
Cabin	Modular Pallet System	Used in the Airbus A400M [41].	9
	OLED Windows	Used extensively in non-aviation fields for e.g. mobile phones and TVs [84].	9
Systems	Foldable Aerodynamic Surfaces	Common in military aviation, for commercial aircraft used with the Boeing 777X [85].	8
	Electric Wheel Hub Motor	Used in several aircraft for demonstrating engine-off taxiing by companies like Germania [86][87].	7
	Retractable Stair	Implemented in the Boeing 737 (operated by RyanAir) [88].	9
	Inspection Drone	First tests carried out (such as Air-Cobot project), further developments in progress has been made by the company Donecle [89].	9
Propulsion	Electric Motor	Used in electric aircraft (CS-23 certified) Extra 330LE [56].	9
	Retractable Propeller	Used in glider aircraft, like on the Akaflieg Berlin B13e prototype [90].	7
	Swept Blade Tips	Used for noise reduction in the Airbus Helicopters H160 preproduction aircraft [72].	8
Powerplant	Lithium Ion Batteries	This technology will be market ready within the five years and is thus rated at a TRL between 7 and 8 [36].	8
	Lithium Ion Capacitor	Mass produced and used for covering peak power demands in electric busses or trams [37].	9

Appendix B Technical Drawing

In the following a technical drawing of MIRUS is provided. All lengths are given in meters.

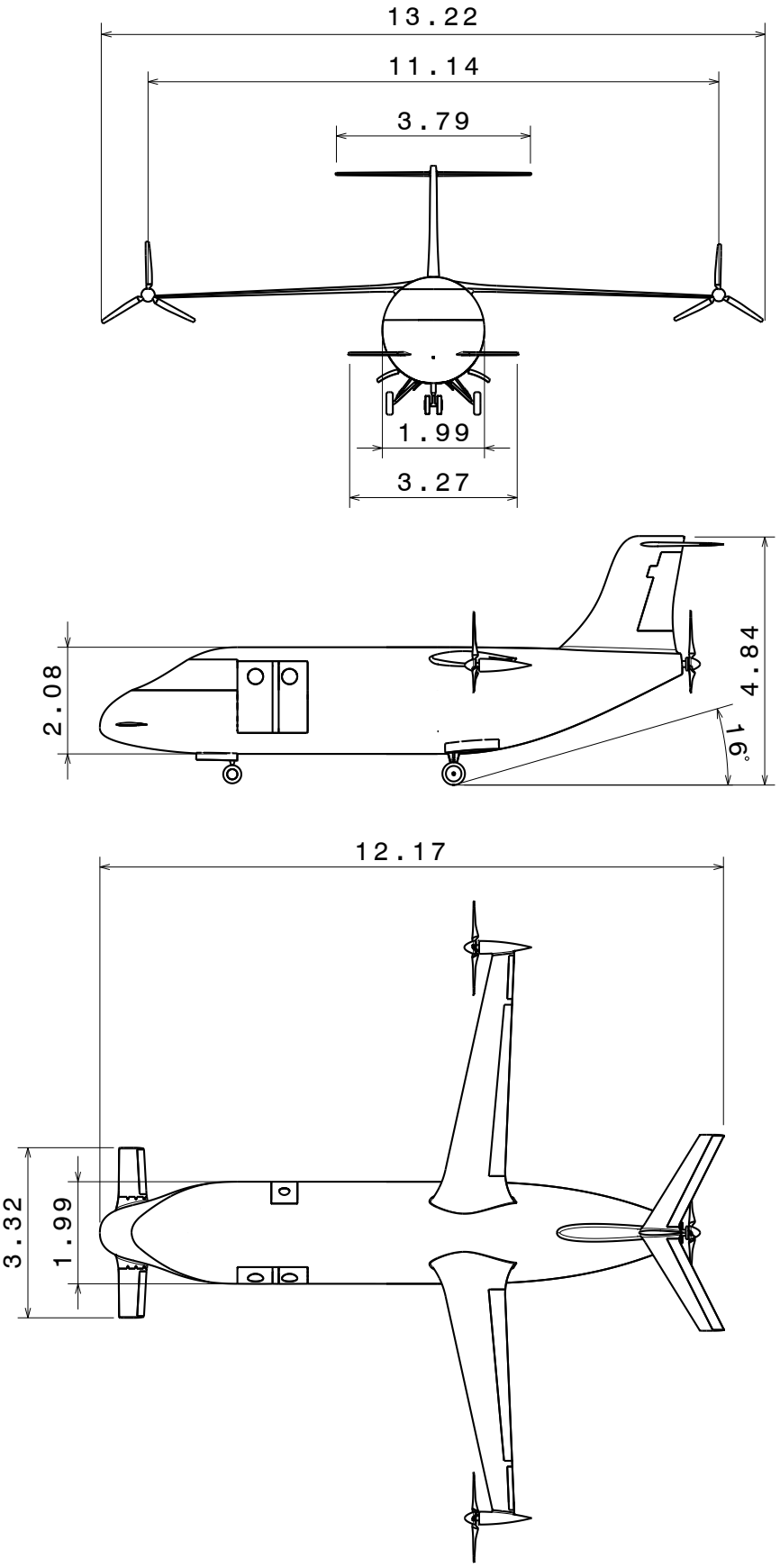

Appendix C Cabin

The following table provides detailed information about the cabin geometries.

Table C.1: Cabin parameters

Parameter	Value in inch
General cabin	
Width	54
Length	154
Height	6
Seat	
Pitch	30
Aisle width	18
Single door	
Width	23
Height	55
Single pallet	
Width	54
Length	51
Height	50

A cross-section view can be found in the following picture.

Figure C.1: Cabin cross-section

Appendix D Autonomy

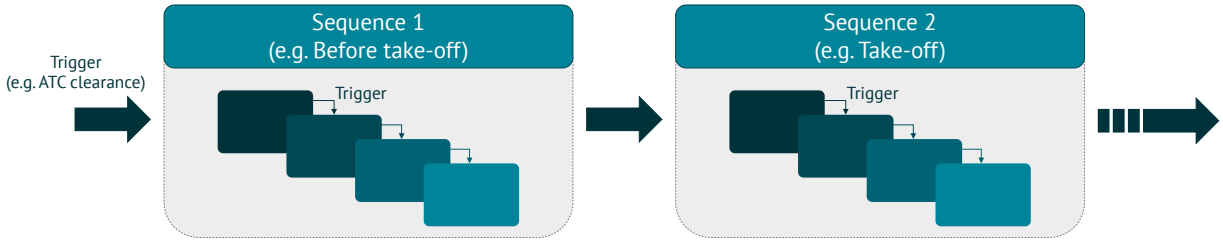

Figure D.1: Cascaded sequence run

Appendix E Powerplant

Figure E.1 and E.2 show the energy consumption and state of charge of each mission segment. As described in Subsection 3.3 the battery's SOC is limited within certain constraints in order to save battery mass. It is noticeable that the SOC of the alternate climb is discharged significantly less than in normal climb. This is due to a reduction of thrust and thus a lower rate of climb since there is no time constraint for the alternates. Hence, more time is spent in the alternate climb and more total energy is consumed. In this case, it is mainly supplied by the generator. All other alternates consume less energy compared to the corresponding regular ones because of the mass loss in the previous segments. The capacitor is always recharged completely in order to ensure a go-around at any landing attempt.

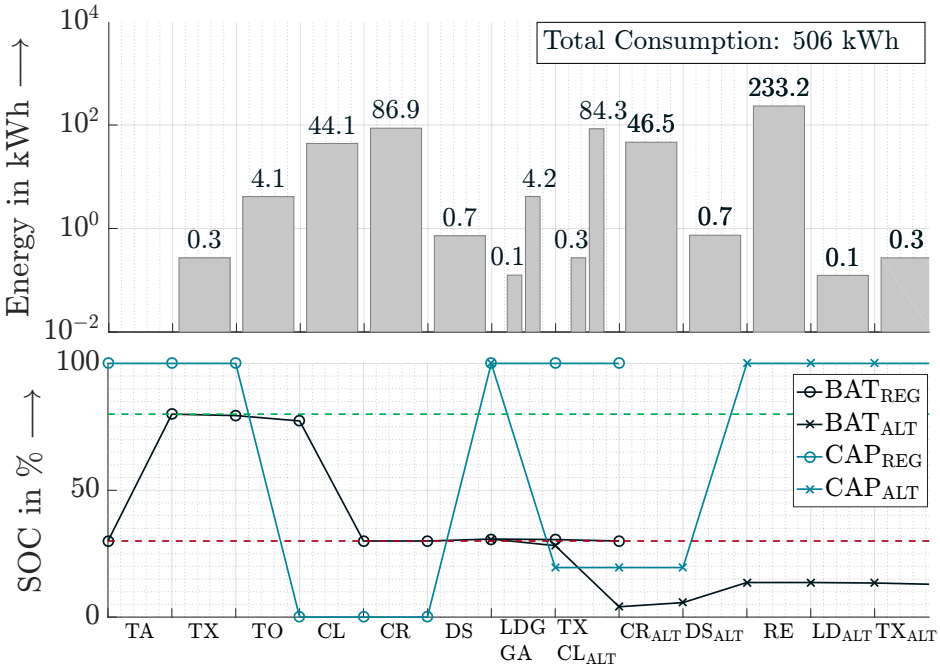

Figure E.1: Energy consumption (above) and SOC (below) for Mission (A)

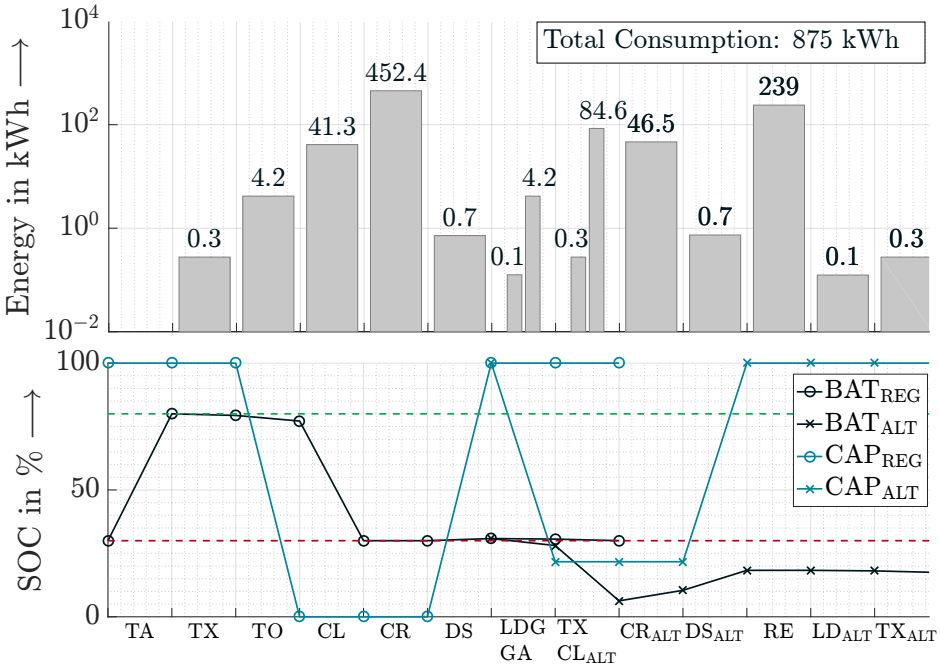

Figure E.2: Energy consumption (above) and SOC (below) for Mission (B)

Appendix F Mass Breakdown

Table F.1: Detailed mass breakdown

MIRUS Mass Breakdown Group Indication		Mass in kg (PAX) (A)	Mass in kg (PAX) (B)	Mass in kg (Cargo) (A)	Mass in kg (Cargo) (B)	% DEW	% MTOM (PAX) (A)	% MTOM (PAX) (B)	% MTOM (Cargo) (A)	% MTOM (Cargo) (B)
Airframe Structure	Wing group	259				12	7	7	7	7
	Horizontal tail group	28				1	1	1	1	1
	Vertical tail group	46				2	1	1	1	1
	Canard wing group	23				1	1	1	1	1
	Fuselage group	348				15	9	9	10	9
	Landing gear	154				6	4	4	4	4
	High-lift devices	168				7	5	4	5	5
	Group total	**1,026**				**44**	**28**	**27**	**29**	**28**
Powerplant	Battery	301				13	8	8	8	8
	Super capacitors	179				8	5	5	5	5
	Gas generator	113				5	3	3	3	3
	Group total	**593**				**26**	**16**	**16**	**16**	**16**
Propulsion Group	Motor (3x) and controller	187				8	5	5	5	5
	Propeller (3x)	40				2	1	1	1	1
	Shaft, nacelle and structure	28				1	1	1	1	1
	Wiring	91				4	2	2	3	2
	Group total	**346**				**15**	**9**	**9**	**10**	**9**
Airframe Services	Instruments, navigational equipment	17				1	1	1	1	1
	Flight control system	76				3	2	2	1	1
	Furnishing and equipment group	43				2	1	1	2	2
	Electronics group	66				3	2	1	1	1
	Air-conditioning and anti-icing group	80				4	2	2	2	2
	Fuel system	38				2	1	1	1	1
	Group total	**320**				**15**	**9**	**8**	**8**	**8**
BASIC EMPTY WEIGHT = DELIVERY EMPTY WEIGHT		**2,285**				**100**	**62**	**60**	**63**	**61**
Operational Items	Crew	85		85			2	2	2	2
	Seating	90		0			2	2	0	0
	Pallet system	150		150			4	3	4	4
	Miscellaneous	3		3			1	1	1	1
	Group total	**328**		**238**			**9**	**8**	**7**	**7**
OPERATIONAL EMPTY WEIGHT		**2,613**		**2,523**			**71**	**68**	**70**	**68**
Payload	Maximum Payload	898		907			24	24	25	24
	Group total	**898**		**907**			**24**	**24**	**25**	**24**
ZERO FUEL WEIGHT		**3,511**		**3,430**			**95**	**92**	**95**	**92**
Fuel	Tripfuel	39	167	38	162		1	4	1	4
	Contingency	2	8	2	8		1	1	1	1
	Alternate	126	129	123	126		3	3	3	3
	Taxi	0	0	0	0		0	0	0	0
	Group total	**167**	**304**	**163**	**296**		**5**	**8**	**5**	**8**
MAXIMUM TAKE-OFF WEIGHT		**3,678**	**3,815**	**3,593**	**3,726**		**100**	**100**	**100**	**100**

Appendix G Data Sheet

Table G.1: Technical data sheet

Parameter	Value
Performance	
Seats	9
Operational range	120 NM
Operational block time	27 min
Maximum range	500 NM
Maximum block time	95 min
Cruise speed	618 $^{km}/_{h}$
Minimum initial cruise altitude	10,000 ft
Cruise glide ratio	20.6
Maximum rate of climb	13.8 $^{m}/_{s}$
Mean flight path angle in descent	-6.3 °
Approach speed	176 $^{km}/_{h}$
Take-off & landing field length	1,000 ft
Maximum wing loading	3,618 $^{N}/_{m^2}$
Installed thrust	19 kN
Geometry	
Overall length	12.17 m
Overall width	13.22 m
Overall height	4.84 m
Wing span	11.1 m
Maximum fuselage diameter	2.08 m
Propeller diameter	2.08 m
Mass	
Maximum payload mass	907 kg
Maximum fuel mass	304 kg
Maximum operating empty mass	2.613 kg
Maximum zero fuel mass	3,511 kg
Maximum take-off mass	3,815 kg

References

[1] M. Ratcliffe. *A Century of Delineating a Changing Landscape: The Census Bureau's Urban and Rural Classification, 1910 - 2010*. U.S. Census Bureau, 2016.

[2] United States Census Bureau (Ed.) *Rural America*. URL: https://gis-portal.data.census.gov/arcgis/apps/MapSeries/index.html?appid=7a41374f6b03456e9d138cb014711e01. (accessed: 09.06.2019).

[3] United States Census Bureau (Ed.) *American Community Survey: 2015*. URL: https://www.census.gov/newsroom/press-releases/2016/cb16-210.html. (accessed: 09.06.2019).

[4] R. A. LaMacchia, R. W. Marx, and J. Sobel. *Geographic Areas Reference Manual (GARM)*. U.S. Department of Commerce, 1994.

[5] D. Kumar. *Rural America is Losing Young People - Consequences and solutions*. URL: https://publicpolicy.wharton.upenn.edu/live/news/2393-rural-america-is-losing-young-people-. (accessed: 09.06.2019).

[6] Alaska Office of Rural Health (Ed.) *Alaska*. URL: https://www.ruralhealthinfo.org/states/alaska. (accessed: 09.06.2019).

[7] Alaska Office of Rural Health (Ed.) *Rural Health Clinics (RHCs)*. URL: https://www.ruralhealthinfo.org/topics/rural-health-clinics. (accessed: 09.06.2019).

[8] H. Lo Wang. *Why The U.S. Census Starts In Alaska's Most Remote, Rural Villages*. URL: https://www.npr.org/2019/01/21/686963414/why-the-u-s-census-starts-in-alaskas-most-remote-rural-villages?t=1560007400599&t=1560081669624. (accessed: 09.06.2019).

[9] U.S. Department of Commerce (Ed.) *Alaska: 2010 Population and Housing Unit Counts*. URL: https://www.census.gov/prod/cen2010/cph-2-3.pdf. (accessed: 14.06.2019).

[10] United Nations (Ed.) *68% of the world population projected to live in urban areas by 2050, says UN*. URL: https://www.un.org/development/desa/en/news/population/2018-revision-of-world-urbanization-prospects.html. (accessed: 09.06.2019).

[11] DSW (Ed.) *Ten countries with the largest population in mid 2018 (in millions)*. URL: https://www.statista.com/statistics/262879/countries-with-the-largest-population/. (accessed: 10.06.2019).

[12] S. Popp. *India's Demographic Transition: Many Chances, but also many Obstacles*. URL: https://www.boell.de/en/2014/06/19/indias-demographic-transition-many-chances-also-many-obstacles. (accessed: 09.06.2019).

[13] S. Popp. *Die neue globale Mittelschicht*. URL: https://www.bpb.de/apuz/196711/die-neue-globale-mittelschicht?p=all. (accessed: 09.06.2019).

[14] S. Bouton, S. M. Knupfer, and I. Mihov. *Urban mobility at a tipping point*. URL: https://www.mckinsey.com/business-functions/sustainability/our-insights/urban-mobility-at-a-tipping-point. (accessed: 10.06.2019).

[15] S. Sinha. *Combating the challenges of urbanization in emerging markets: Lessons from India*. URL: https://www.mckinsey.com/industries/capital-projects-and-infrastructure/our-insights/combating-the-challenges-of-urbanization-in-emerging-markets-lessons-from-india. (accessed: 10.06.2019).

[16] United Nations (Ed.) *Sustainable Development Goals - 17 Goals to Transform Our World*. URL: https://www.un.org/sustainabledevelopment/. (accessed: 18.06.2019).

[17] W. F. Laurance and A. Balmford. *Ein weltweiter Straßenplan*. URL: https://www.spektrum.de/kolumne/ein-weltweiter-strassenplan/1189365. (accessed: 09.06.2019).

[18] R. Dobbs, J. Remes, and F. Schaer. *Unlocking the potential of emerging-market cities*. URL: https://www.mckinsey.com/featured-insights/urbanization/unlocking-the-potential-of-emerging-market-cities. (accessed: 10.06.2019).

[19] J. Rossant. *The urban mobility revolution is here*. In: Cities Today, Mar. 2018.

[20] D. Michaels T. Enders B. Piccard. *Highlights - Up in the Air! Vision & Reality (Enders, Piccard, Michaels) | DLD17*. Youtube. 2017. URL: https://www.youtube.com/watch?time_continue=158&v=vE22YmPIVQg=1m40s.

[21] Bauhaus Luftfahrt e.V. (Ed.) *CentAirStation" airport concept and CityBird aircraft concept*. URL: https://www.bauhaus-luftfahrt.net/en/topthema/centairstation-and-citybird/. (accessed: 10.06.2019).

[22] D. Megginson. *Our Airports - open Data Download*. URL: http://ourairports.com/data/. (accessed: 24.06.2019).

[23] Ministry of Defence of the UK (Ed.) *Turbine Fuel, Aviation Kerosine Type, Jet A-1*. URL: https://webarchive.nationalarchives.gov.uk/20100814170713/http%3A//www.dstan.mod.uk/standards/defstans/91/091/00000600.pdf. (accessed: 22.06.2019).

[24] Global Aviation Navigator Inc. (Ed.) *GlobalAir Fuelmaps*. URL: https://www.globalair.com/airport/fuelmap.aspx?aptcode=LAX&av=pu&rad=100&FacType=Airport&rwy=any&fueljeta=true. (accessed: 29.06.2019).

[25] A. K. Fields M. A. Rapino. *Mega Commuters in the U.S.* Baltimore: United States Census Bureau, 2013.

[26] Western Aircraft (Ed.) *Western Aircraft launches Pilatus one day, 100 hour inspections*. URL: https://www.westair.com/western-aircraft-launches-pilatus-one-day-100-hour-inspections/. (accessed: 30.06.2019).

[27] M. Whalley. *Lessons from The V/STOL Wheel of Misfortune*. URL: https://passerineaircraft.com/lessons-from-the-vtol-circle-of-misfortune-821/. (accessed: 19.06.2019).

[28] C. C. Rossow, K. Wolf, and P. Horst. *Handbuch der Luftfahrzeugtechnik*. München: Carl Hanser Verlag, 2014.

[29] S. Gudmunsson. *General Aviation Aircraft Design: Applied Methods and Procedures*. Oxford: Elsevier, 2014.

[30] E. R. Kendall. *The Aerodynamics of Three-Surface Airplanes*. URL: https://arc.aiaa.org/doi/pdf/10.2514/6.1984-2508. (accessed: 14.05.2019).

[31] L.M. Nicolai. *Fundamentals of aircraft and airship design*. Reston: American Institue of Aeronautics and Astronautics, Inc., 2010.

[32] Yunchao Yang and Gecheng Zha. *Super-Lift Coefficient of Active Flow Control Airfoil: What is the Limit?* Dept. of Mechanical and Aerospace Engineering University of Miami, 2017.

[33] R. Berger. *Aircraft Electrical Propulsion – Onwards and Upwards*. Roland Berger GmbH, London, 2018.

[34] M. Hepperle. *Electric Flight – Potential and Limitations*. URL: https://elib.dlr.de/78726/1/MP-AVT-209-09.pdf. (accessed: 25.04.2019).

[35] R. Berger. *Aircraft Electrical Propulsion – The Next Chapter of Aviation?* URL: https://www.rolandberger.com/de/Publications/New-developments-in-aircraft-electrical-propulsion-(CH).html. (accessed: 19.05.2019).

[36] M. Meeus. *Overview of Battery Cell Technologies*. URL: https://europa.eu/sinapse/webservices/dsp_export_attachement.cfm?CMTY_ID=0C46BEEC-C689-9F80-54C7DD45358D29FB&OBJECT_ID=230DABFD-90AB-8F7D-083EF5BD909DD025&DOC_ID=9C5B91FE-01BC-5F72-79D01E1939A9EE53&type=CMTY_CAL. (accessed: 29.04.2019).

[37] N. Omar et al. *Lithium-Ion Capacitor - Advanced Technology for Rechargeable Energy Storage Systems*. In: World Electric Vehicle Journal, Sept. 2013.

[38] J.Ludowicy et al. *Sizing Studies of light aircraft with serial hybrid propulsion systems*. FH-Aachen, Institute of Aircraft Engineering, 2018.

[39] S. Nootebos. *Aerodynamic analysis and optimisation of wingtip-mounted pusher propellers*. URL: https://repository.tudelft.nl/islandora/object/uuid%5C%3A83c88c41-3fa0-4ddb-9cc2-b5e574d0cd6a. (accessed: 19.05.2019).

[40] F. Persiani S. Bagassi F. Lucchi. *Aircraft Preliminary Design: a windowless concept*. 5th CEAS Air and Space Conference, 2015.

[41] G. Martin. *Airbus Reveals New Modular Cabin Concept That Could Change How We Fly*. URL: https://www.forbes.com/sites/grantmartin/2016/12/14/airbus-reveals-new-modular-cabin-airplane-concept/#2e057b71345f. (accessed: 24.06.2019).

[42] E. Fleuti and C. Ruf. *Aircraft Ground Energy Systems*. Zurich, Swiss, 2018.

[43] IHGC Innovators (Ed.) *Future of Ground Handling Industry - Big Idea*. Montreal Canada, IATA, 2019.

[44] E. A. Ginten. *Pilotenmangel bremst die Weltwirtschaft*. URL: https://www.welt.de/wirtschaft/article1444023/Pilotenmangel-bremst-die-Weltwirtschaft.html. (accessed: 23.06.2019).

[45] Handelsblatt (Ed.) *Anteil der Personalkosten an den Gesamtkosten ausgewählter Fluggesellschaften im Geschäftsjahr 2014*. URL: https://de.statista.com/statistik/daten/studie/460592/umfrage/fluggesellschaften-anteil-der-personalkosten-an-den-gesamtkosten/. (accessed: 23.06.2019).

[46] D. Tost. *Airbus Aims for Self-flying Car Takeoff in 2017*. URL: https://www.handelsblatt.com/today/companies/ceo-plans-airbus-aims-for-self-flying-car-takeoff-in-2017/23565408.html?ticket=ST-4464526-WVJmIex4CuCKnxafQX4n-ap1. (accessed: 23.06.2019).

[47] National Research Council (Ed.) *Autonomy Research for Civil Aviation: Toward a New Era of Flight*. Washington DC: The National Academies Press, 2014. ISBN: 978-0-309-30614-0. DOI: 10.17226/18815. URL: https://www.nap.edu/catalog/18815/autonomy-research-for-civil-aviation-toward-a-new-era-of.

[48] L. Downes. *The Laws of Disruption - Harnessing the New Forces that Govrern Life and Business in the Digital Age*. New York: Basic Books, 2009. ISBN: 978-0-465-01864-2.

[49] J. Castle and C. Fornaro. *Flying solo - how far are we down the path towards pilotless planes?* UBS Q-Series, 2017.

[50] Y. Lim et al. *Commercial Airline Single-Pilot Operations: System Design and Pathways to Certification*. IEEE Aerospace and Electronic Systems Magazine, 2017.

[51] W. Bellamy III. *Europe's Aircraft Data Link Service Network is Improving*. URL: https://www.aviationtoday.com/2018/09/27/europes-aircraft-data-link-service-network-improving/. (accessed: 23.06.2019).

[52] Airbus Industries (Ed.) *Airbus A380 - Flight Crew Operating Manual*. Airbus, 2012.

[53] D. Siegel. *Development of an Autoland System for General Aviation*. Aurora Flight Science, 2012.

[54] F. Pinchetti et al. *FlySmart - Automatic Take-Off and Landing of an EASA CS-23 Aircraft*. University of Stuttgart, 2016.

[55] Emrax d.o.o. (Ed.) *Technical Data and Manual for EMRAX Motors/Generators*. URL: https://emrax.com/wp-content/uploads/2017/10/user_manual_for_emrax_motors.pdf. (accessed: 30.06.2018).

[56] Siemens AG (Ed.) *Factsheet Rekord-Motor SP260D und Extra 330LE*. URL: https://www.siemens.com/press/pool/de/feature/2015/corporate/2015-03-electromotor/factsheet-erstflug-weltrekordmotor-d.pdf. (accessed: 30.06.2018).

[57] Hamilton Std. (Ed.) *Generalized Method of Propeller Performance Estimation 1961-1963*. Windsor Locks: Hamilton Standard Division, 1963.

[58] F. W. Diederich. *A simple approximate method for calculating spanwise lift distributions and aerodynamic influence coefficients at subsonic speed*. Langley: National Advisory Committee for Aeronautics, 1952.

[59] R. Radespiel et al. *Active flow control for high lift with steady blowing*. Institute of Fluid Mechanics Technische Universität Braunschweig Braunschweig Germany, 2016.

[60] N. Beck, T. Landa, and A. Seitz. *Drag Reduction by Laminar Flow Control*. In: MDPI energies, Vol 99, Jan. 2018, p. 14. DOI: 10.3390/en11010252.

[61] S. H. Teichel et al. *Design considerations for the components of electrically powered active high-lift systems in civil aircraft*. Deutsches Zentrum für Luft- und Raumfahrt e.V., 2015.

[62] Marco Burnazzi. *Design of Efficient High-Lift Configurations with Coanda Flaps*. TU Braunschweig Institut für Strömungsmechanik Germany, 2016.

[63] J. P. Campbell and Marion O. McKinney. *Summary of methods for calculating lateral stability and response and for estimating lateral stability derivates*. NACA, 1952.

[64] R. Luckner. *Skript zur Lehrveranstaltung Flugmechanik II*. Berlin: TU Berlin, 2016.

[65] B. Xu et al. *Modeling of Lithium-Ion Battery Degradation for Cell Life Assessment*. In: IEEE Transactions on Smart Grid, Vol 99, June 2016, pp. 1–1. DOI: 10.1109/TSG.2016.2578950.

[66] X. Luo et al. *Overview of current development in electrical energy storage technologies and the application potential in power system operation*. In: Applied Energy, Oct. 2014. DOI: 10.1016/j.apenergy.2014.09.081.

[67] D. P. Raymer. *Aircraft design: a conceptual approach*. Sylmar: American Institute of Aeronautics and Astronautics, 1989. ISBN: 9780930403515.

[68] G. D. Häberle et al. *Tabellenbuch Elektrotechnik: Tabellen, Formeln, Normenanwendungen*. Haan: Europa-Lehrmittel, 2015.

[69] D. G. Simons. *Introduction to Aircraft Noise*. Delft: Delft University of Technology, 2017.

[70] P. Guyer. *An Introduction to Sound Level Data for Mechanical and Electrical Equipment*. URL: https://www.cedengineering.com/userfiles/Intro%5C%20to%5C%20Sound%5C%20Level%5C%20Data%5C%20for%5C%20Mech%5C%20&%5C%20Elec%5C%20Equip.pdf. (accessed: 01.06.2019).

[71] J. J. Berton and D. M. Nark. *Low-Noise Operating Mode for Propeller-Driven Electric Airplanes*. NASA, 2018.

[72] M. Colognes. *The new blue edge concept*. In: Rotor Journal, Apr. 2010.

[73] R. W. Hess and H. P. Romanoff. *Aircraft Airframe Cost Estimating Relationships*. RAND Cooperation, 1987.

[74] C. N. Eastlake and H. W. Blackwell. *Cost Estimating Software for General Aviation Aircraft Design*. Embry-Riddle Aeronautical University/Lockheed Martin Corporation, 2000.

[75] C. Laslau. *Crossing the Line: Li-ion Battery Cost Reduction and Its Effect on Vehicles and Stationary Storage*. Lux Research, 2015.

[76] K. Bullis. *Ultracapacitors to Boost the Range of Electric Cars*. URL: https://www.technologyreview.com/s/423914/ultracapacitors-to-boost-the-range-of-electric-cars/. (accessed: 05.05.2019).

[77] Association of European Airlines (Ed.) *Short-Medium Range Aircraft AEA Requirements*. AEA, 1989.

[78] F. Gomez and D. Scholz. *Improvements to ground handling operations and their benefits to direct operating costs*. HAW Hamburg, 2009.

[79] FAA (Ed.) *Economic Values for FAA Investment and Regulatory Decisions Guide - Section 4*. FAA, 2016.

[80] Piaggio Aerospace S.p.A. (Ed.) *Avanti Evo - Specification and Design*. Piaggio Aerospace, 2016.

[81] J. Gertler. *V-22 Osprey Tilt-Rotor Aircraft: Background and Issues for Congress*. Congressional Research Service, 2011.

[82] J.H. Nichols and M.J. Harris. *Fixed wing aerodynamics with and without supplementary thrust deflection*. NASA, 2013.

[83] Airbus S.A.S. (Ed.) *Airbus technical maganzine (June 2013) - Special Edition A350 XWB*. Airbus, 2013.

[84] Metalgrass Ltd. (Ed.) *An introduction to OLED displays*. URL: `https://www.oled-info.com/oled-introduction`. (accessed: 25.06.2019).

[85] J. Ostrower. *Beyond the carrier deck: A glimpse at the 777X flding wingtip*. URL: `https://theaircurrent.com/dispatches/beyond-the-carrier-deck-a-glimpse-at-the-777x-folding-wingtip/`. (accessed: 25.06.2019).

[86] M. Whalley. *Lessons from The V/STOL Wheel of Misfortune*. URL: `https://www.stirling-dynamics.com/news/stirling-redesigns-wheel/`. (accessed: 19.06.2019).

[87] S. Cash, Q. Zhou, and O. Olatunbosun. *Development of a series hybrid electric aircraft push-back vehicle*. Department of Mechanical Engineering, University of Birmingham, 2018.

[88] F. Gomez and D. Scholz. *Aircraft Design for Low-Cost Ground Handling*. Hamburg University of Applied Sciences, 2009.

[89] M. Bauda, A. Grenwelge, and S. Larnier. *3D scanner positioning for aircraft surface inspection*. Department of Systems Engineering and Operations Research, Toulouse, 2018.

[90] Akaflieg Berlin e.V. (Ed.) *Das ist die B13e*. URL: `https://b13e.akaflieg-berlin.de/bestandteile/`. (accessed: 25.06.2019).

Deutsches Zentrum
DLR für Luft- und Raumfahrt

Formular zur Freigabe der eingereichten Arbeit
[NASA/DLR-Design Challenge 2019]

Titel der eingereichten Arbeit	MIRUS	
Einreichende Person mit Studiengang	Yannic Cabac	(Luft- und Raumfahrttechnik)
Andere Teammitglieder mit Studiengang	Ramón Beck	(Verkehrswesen)
	Jiri Dehmel	(Luft- und Raumfahrttechnik)
	Felix Fritzsche	(Luft- und Raumfahrttechnik)
	Lennart Kracke	(Verkehrswesen)
	Kevin Lehnhardt	(Luft- und Raumfahrttechnik)
	Kristof Miertsch	(Verkehrswesen)
	Stephanie Roscher	(Verkehrswesen)
	Roman Uzun	(Luft- und Raumfahrttechnik)
	Ai Quynh Vo	(Luft- und Raumfahrttechnik)
Betreuer des Lehrstuhls	Andreas Gobbin, MSc.	

Lehrstuhl	Fachgebiet Luftfahrzeugbau und Leichtbau, TU Berlin		
Adresse des Lehrstuhls	Marchstr. 12-14		
PLZ, Ort	10587 Berlin	**Telefon**	+49 (30) 314 - 28538

Ich bestätige hiermit, dass die oben genannte Einreichung einschließlich Text, Illustrationen und Zusatzmaterial durch den genannten Studierenden bzw. das Team des genannten Studierenden erstellt, nicht aus einer anderen Arbeit, Fotografie, Illustration oder Webseite kopiert oder von einer anderen Person erstellt wurde. Mir ist bekannt, dass die Einreichung einschließlich Text, Illustrationen und Zusatzmaterial nicht zurückgegeben wird. Ich erteile hiermit dem Deutschen Zentrum für Luft- und Raumfahrt (DLR) die nicht exklusive Erlaubnis, die eingereichte Arbeit einschließlich Text, Illustrationen und Zusatzmaterial sowie den Namen, das Foto, die Hochschule und den Abschluss/Studienstand des/der Studierenden für alle dem DLR geeignet erscheinenden Zwecke und Formen der Veröffentlichung zu verwenden, zu vervielfältigen, Teile zu veröffentlichen, in Kopie der Öffentlichkeit zugänglich zu machen und öffentlich zu präsentieren. Das DLR kann die Einreichung einschließlich Text, Illustrationen und Zusatzmaterial über verschiedene Medien veröffentlichen; dazu gehören unter anderem Druck, Fernsehen, Webseiten oder andere Medien jedweder Art. Das DLR kann es auch Dritten gestatten, die Rechte des DLR zur nicht exklusiven Veröffentlichung auszuüben; dazu gehören unter anderem das Recht zur Präsentation oder zur Veröffentlichung der gesamten Arbeit einschließlich Text, Illustrationen und Zusatzmaterial auf eine Art und Weise, die dem DLR geeignet erscheint. Falls die eingereichte Arbeit Informationen aus Gesprächen mit Peers, Eltern oder anderen enthält, ist der Studierende dafür verantwortlich, die zur Verwendung besagter Informationen erforderlichen Genehmigungen gemäß den vorliegenden Bestimmungen einzuholen. Sämtliche Rechte an der Nutzung der Inhalte der Einreichung verbleiben bei den Urhebern.

Y. Cabac

Yannic Cabac

TECHNISCHE UNIVERSITÄT BERLIN
Institut für Luft- und Raumfahrt
FG Luftfahrzeugbau und Leichtbau
Sekr. F2
Marchstraße 12-14 • D-10587 Berlin

Prof. Dr.-Ing. Andreas Bardenhagen